CrossMark

Lane dynamics in pair-ion plasmas: effect of obstacle and geometric aspect ratio

Swati Baruah [1],†, **Vishal K. Prajapati** [1] and **R. Ganesh** [2]

[1]The Assam Kaziranga University, Jorhat-785 006, Assam, India

[2]Institute for Plasma Research, Bhat, Gandhinagar 382428, Gujarat, India

Lane formation dynamics of driven two-dimensional pair-ion plasmas is investigated in under-damped cases where the effect of particle inertia cannot be neglected. Extensive Langevin dynamics simulations using an OpenMP parallel program are carried out to analyse the effect of obstacle and geometric aspect ratio on lane formation dynamics previously reported in Sarma *et al.* (*Phys. Plasmas*, vol. 27, 2020, 012106) and Baruah *et al.* (*J. Plasma Phys.*, vol. 87, 2021, 905870202). Lanes are found to form when like particles move along or opposite to the applied field direction. Lane order parameter, cumulative order parameter and distribution of the order parameter have been implemented to detect phase transition. The effect of geometric aspect ratio on the stability of lanes is systematically determined in both the presence and absence of an obstacle. Here, a specular reflective boundary condition is implemented to mimic an obstacle. We demonstrate that an obstacle promotes the merging of lanes, and the system gradually transitions to a partially mixed phase with higher value of aspect ratio. The occurrence of lane mixing phenomena at the separation boundary of two oppositely flowing lanes at higher value of aspect ratio is observed. In the presence of an oscillatory electric field, the lane merging tendency is reduced to a large extent as compared to the system where a constant electric field is applied. Furthermore, in the presence of both space- and time-varying electric fields, an appearance of a void is observed on either side of the obstacle. The study finds that the presence of an external magnetic field promotes acceleration of the phase transition process towards the lane mixing phase; it also reveals the existence of electric field drift in the system. Our findings may prove to be useful in understanding the nature of lane dynamics in naturally occurring pair-ion plasma systems as well as their relevance to technological applications that exploit or mitigate self-organization.

1. Introduction

In recent years, much interest has grown in the field of pair-ion plasmas (PIPs), which are composed of two ion components with equal mass and opposite charges. A criterion to define the pure PIP was presented in 2007 (Saleem 2007). In that work, it was shown that the simplest form of this criterion to define the produced plasma as pure PIP is that the electron plasma oscillation frequency (ω_{pe}) and the positive ion plasma oscillation

† Email address for correspondence: baruah.s1@gmail.com

frequency (ω_{p+}) should obey the relation $\omega_{pe} << \omega_{p+}$. If this condition holds, only then one can assume that the electrons have a negligible role in the plasma dynamics. The PIP is expected to be used for the synthesis of dimers (Oohara & Hatakeyama 2003) directly from carbon allotropes, as well as for nanotechnology (Shukla & Stenflo 2005). The physics of PIPs has grown into a broader and vibrant field of research and investigation as its applications vary from astrophysical scales to the terrestrial laboratory. Recently, a method for generating pure PIP has been developed. A PIP without electrons is generated using fullerene (C_{60}) as an ion source through the processes of hollow-electron-beam impact ionization (Oohara, Date & Hatakeyama 2005). This gave rise to a unique possibility of investigating the collective behaviour of a PIP experimentally under controlled conditions. In a very recent study Oohara *et al.* (2019) pointed out that the criterion presented in 2007 (Oohara & Hatakeyama 2007) to define a pure PIP (Saleem 2007) has not been achieved, although the electron density in this plasma has been estimated to be $n_{e0}/n_{+0} < 10^{-2}$, where n_{e0} and n_{+0} are the equilibrium electron and positive ion densities, respectively. The results of Oohara & Hatakeyama (2007) are also discussed by Chen (2016) in his famous book on plasma physics. Furthermore, a negative ion plasma with mass $m_- \approx 10m_+$ (where m_+ is the mass of a positive ion) and a very low residual electron content ($n_e/n_+ < 10^{-4}$, where n_e and n_+ represent the electron and positive ion densities, respectively) has been produced in a Q machine by electron attachment to C_7F_{14} at a pressure 10^{-5} Torr (Kim & Merlino 2007).

Vladimirov *et al.* (2003) studied ion acoustic waves (IAW) in a low-temperature plasma containing dust particles and negative ions. Verheest (2006) suggested that the IAW can be excited in pure PIP if the temperatures of positive and negative ions are different, i.e. $T_+ \neq T_-$, while experimenters mentioned that these temperatures were almost equal $T_+ \doteq T_-$ (Oohara *et al.* 2005). A few authors expressed that the observation of IAW in the plasma indicates the presence of electrons in the system and hence experimenters should confirm the ratio of electron to positive ion densities to ignore electron dynamics (Saleem, Vranjes & Poedts 2006). They used quasi-neutrality in the investigation of IAW in pair ion electron plasma. Later on (Saleem 2006), it was pointed out that quasi-neutrality is not a good approximation to be used in pair ion electron plasma because when the electron density is reduced, then the electron Debye length becomes very large, i.e. $1 << \lambda_{De}^2 k^2$, where λ_{De} is the electron Debye length and k is the wave vector. Then it was stressed that there should be a rigorous criterion to define a pure PIP. Mahajan & Shatashvili (2008) investigated the nonlinear propagation of high-intensity electromagnetic waves in a PIP. Vranjes & Poedts (2005) reported that electrons might be added to a PIP to study their effects on the plasma stability. Tribeche *et al.* (2007) studied electrostatic solitary structures in a charge-varying dusty PIP. Recently, Arshad & Mahmood (2010) investigated electrostatic ion waves in a non-Maxwellian PIP. Abdelsalam (2010) studied the nonlinear properties of the dust-IAW in a collision-less dense PIP. Kim, Heinrich & Merlino (2008) investigated experimentally the excitation of electrostatic ion cyclotron waves in a plasma consisting of K^+ ions, electrons and $C_7F_{14}^-$ negative ions, and the experimental results were found to be in general agreement with the three-fluid model of electrostatic ion cyclotron waves in a negative ion plasma. Very recently, Kim *et al.* (2013) also performed an experimental investigation of low-frequency electrostatic waves ($<<$ ion gyro-frequency) in a plasma containing light positive and heavy negative ions ($m_- 10m_+$) and a small concentration of electrons, where the wave properties were found consistent with a density-gradient-driven drift wave instability in a nearly electron-free, positive ion–negative ion plasma. On the other hand, Baruah, Ganesh & Avinash (2015) carried out a study of the phase stability of PIPs in the strongly coupled regime, where an interesting phase coexistence between liquid-like and vapour-like phases has been observed. Additionally, our recent work on a self-organization

effect (Sarma, Baruah & Ganesh 2020) shows the formation of non-equilibrium lane formation phenomena in naturally occurring PIP systems. Furthermore, very recently we have also studied lane formation dynamics in an externally driven PIP system, where a peculiar lane formation–disintegration parameter space is identified in the presence of an external magnetic field (Baruah, Sarma & Ganesh 2021).

Pattern formation in PIPs also has been a long-standing, intriguing topic. The dissipative interactions through friction are a source of nonlinear dynamics and complexity which result in pattern formation on large scales. Lane formation is an evolving pattern formation that occurs when two species of particles are driven into each other. The formation of lanes is a ubiquitous phenomenon occurring in nature, where an originally homogeneous mixture of particles moving in opposite directions segregates into macroscopic lanes composed of different species. Typically, the lanes exhibit a considerably anisotropic structural order accompanied by an enhancement of their mobility. The phenomenon is most commonly known from pedestrian dynamics in highly populated pedestrian zones (Feliciani, Murakami & Nishinari 2018). Specifically, when two groups of elements are moving in opposite directions, the agents of the same species tend to move collectively and eventually form a lane in the driven direction. This structure formation is closely related to how efficiently pedestrians can flow towards a desired direction in various crowded environments, such as evacuation in the event of a disaster. This disordered–ordered transition of particles is due to the ability to tailor the interactive forces between the particles which provides a fertile ground for understanding the fundamental aspects of phase transition behavioor. In fact, the self-consistent phase transition occurs when particle correlation force effects become significantly large (Dwivedi 2000). Similar situations with two groups of particles moving in opposite directions have been extensively studied in the context of lane and pattern formations in different model systems of driven particles, such as colloidal dispersions (Vissers, van Blaaderen & Imhof 2011*a*; Vissers *et al.* 2011*b*; Tarama, Egelhaaf & Löwen 2019), lattice gases (Schmittmann & Zia 1998), molecular ions (Netz 2003), microswimmers (Kogler & Klapp 2015) and plasmas (Sarma *et al.* 2020; Baruah *et al.* 2021). Although several works have already been performed concerning non-equilibrium conditions that form patterns or exhibit complex, perhaps chaotic behaviours, the mechanisms of pattern formation for non-equilibrium conditions are much less clear and are an active area of research. Additionally, a fundamental understanding of such non-equilibrium phenomena requires the study of non-equilibrium phase transition phenomena from a 'first principles' approach. For a given interaction potential, a classical molecular dynamics simulation is a 'first principles' approach which integrates an N-particle system without any assumptions (Sarma *et al.* 2020; Baruah *et al.* 2021).

As mentioned above, as a field of research, non-equilibrium physics is inherently interdisciplinary and several studies in the context of lane formation have already been performed, but using a bulk system without obstacles. In this work we report on comprehensive simulation studies of lane formation in a PIP system using Langevin dynamics simulation. More specifically, we investigate the effect of obstacle and geometric aspect ratio on lane formation dynamics, which, to the best of our knowledge, has never been addressed before. Here, the entire work is performed for $\kappa \sim 0$ ($\kappa = 10^{-4}$) and number density $\rho = 1.0$, where $\kappa = a/\lambda_D$ is the screening parameter resulting from the shielding dynamics of 'background' charged particles, λ_D is the Debye length and a is the Wigner–Seitz radius, and for the rest of the presentation these values of κ and ρ are used. The study has been performed in the presence of both constant and time-varying external electric fields in the under-damped limit. Here, in order to detect the transition towards lane formation, a lane order parameter (ϕ), cumulative order parameter (ϕ') and

occurrence distribution function of ϕ ($f(\phi)$) are used. Our study shows that, as expected (Sarma *et al.* 2020), on application of constant external field with field strength E_0 greater than a critical threshold value E_c, a state of lane formation is achieved. The study also reveals that increasing the aspect ratio in such a situation tends to decrease ϕ values. This is because at higher aspect ratio values the individual lanes of same species merge together for a better flow efficiency resulting in two separate lanes for individual species of the PIP system. Interestingly, it is also observed that with the introduction of a specular reflective boundary condition (SRBC) like an obstacle, the lane merging tendency is introduced at a lower value of aspect ratio. Additionally, a comparative analysis of the simulation results shows that higher values of aspect ratio and the presence of an obstacle are found to have a tendency to decrease the stability of the lanes by decreasing ϕ values below the critical value of ϕ (i.e. $\phi = 0.5$, where the system begins to form lanes), indicating the existence of a partially mixed phase even in the presence of an external field with strength $E_0 \geq E_c$. The study also reveals that the lane stability decreases for geometric aspect ratio value $L_y/L_x \geq 9$ in the presence of an obstacle. In the second part of the paper we discuss the influence of the obstacle and geometric aspect ratio on lane formation dynamics in a PIP system in the presence of an oscillatory electric field. It is observed that in the presence of an oscillatory electric field, the lane merging tendency is reduced as compared to the system where a constant electric field is applied even at higher aspect ratios. We also report the formation of a low-density region might be treated as a void on either side of the obstacle in the presence of both space- and time-varying electric fields. This study has allowed us to discuss several interesting similarities and differences between constant and oscillatory field lane formation dynamics of these systems in both the presence and absence of an external magnetic field. Although pure electron-free plasma has not been created in the laboratory so far, we perform numerical simulations for a two-dimensional (2-D) pure PIP which may be useful for future investigations on this topic.

The rest of the paper is organized as follows. In § 2, we define the model used, the simulation technique along with the SRBC. The simulation procedure and the diagnostic techniques are discussed in § 3. In § 4, the results are presented and discussed in detail. Finally we finish with conclusions in § 5.

2. The model

We simulate the Langevin dynamics for a 2-D PIP system of N charged particles of the same magnitude $|Q|$ and of equal masses in a simulation box having dimensions L_x, L_y. In this model, each particle is assigned either positive or negative charge. Half of the particles carry positive charge and the other half carry negative charge, with partial number densities $\rho_1 = \rho_2$ giving $\rho_1 + \rho_2 = \rho$, where $\rho = N/L_xL_y$ is the number density of the system. The periodic boundary condition is used in outer walls of the simulation chamber in both x and y directions. Here, as shown in figure 1, we have designed a SRBC (Piran 2005) which mimics an 'obstacle' that is placed at the centre of the simulation box. The SRBC allows the reflection of a particle from a wall back into the simulation box (see figure 1). Specular reflection is a mirror-like reflection where the angle of reflection θ_r is equal to the angle of incidence θ_i. In a specular reflection, the normal velocity of the particle is reversed, the tangential velocity is retained and the energy is preserved. The specularly reflecting boundary is representative of a 'mooth' wall that does not offer any resistance to the particle flow (Feliciani *et al.* 2018). Figure 1 illustrates the specular reflection of particles (inside the simulation chamber) from an 'obstacle' with specular reflection walls.

In this paper, we extend the set-up previously studied in Sarma *et al.* (2020) and Baruah *et al.* (2021) in the following directions. First, we study – in both the presence and absence
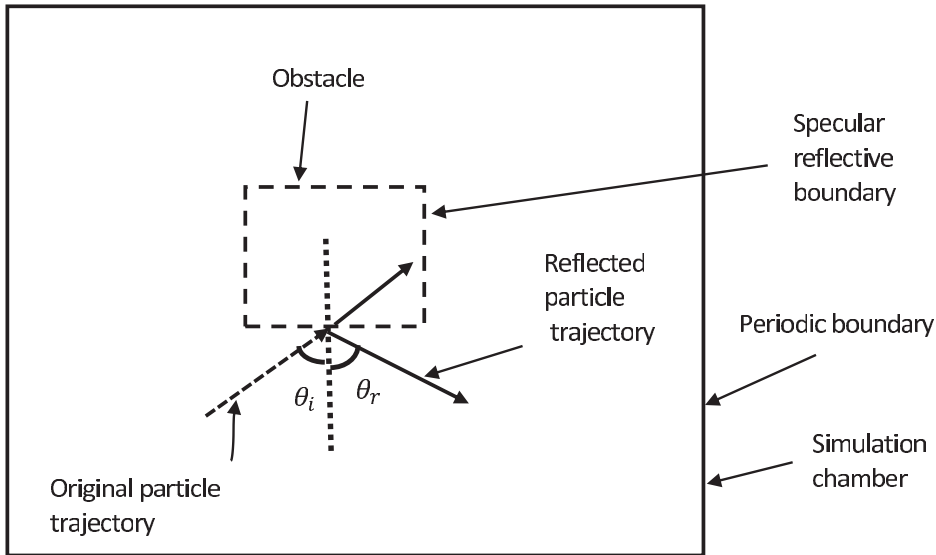
FIGURE 1. A schematic illustrating specular reflection of particles from an 'obstacle' placed in the centre of the simulation domain.

of an obstacle – the case where thee effect of geometric aspect ratio is observed. Second, we study – for the obstacle and geometric aspect ratio – the case where an external magnetic field is applied. Therefore, for the sake of continuity of discussion, again we are presenting the same model as used in our previous studies (Sarma *et al.* 2020; Baruah *et al.* 2021).

The particle trajectories are governed by the Langevin dynamics:

$$m_i \frac{\mathrm{d}^2 \boldsymbol{r}_i}{\mathrm{d}t^2} = -\gamma \frac{\mathrm{d}\boldsymbol{r}_i}{\mathrm{d}t} - \sum_{i<j} \nabla U\left(r_{ij}\right) + \boldsymbol{F}_{ext} + \boldsymbol{F}_i^{(R)}, \qquad (2.1)$$

where $i = 1, \ldots, N$, m_i and r_i are, respectively, the number of PIP particles and the mass and position of the ith particle, γ represents the friction coefficient that produces a non-conservative, non-systematic force induced by the background interaction (e.g. frictional forces) and the random force $\boldsymbol{F}_i^{(R)}$ is related to the fluctuation of the collisions, and normally that is often assumed to be a Gaussian distribution with zero mean. The term $-\gamma (\mathrm{d}\boldsymbol{r}_i/\mathrm{d}t)$ always points opposite to the velocity $\mathrm{d}\boldsymbol{r}_i/\mathrm{d}t$, so it tends to slow down a particle. If it were the only term, it would lead to exponentially decaying velocity. However, the term $\boldsymbol{F}_i^{(R)}$ prevents that from happening by constantly applying random kicks to the particles. Essentially, there is one term that removes energy and one term that adds energy. When the system is in statistical equilibrium, the two terms will roughly balance out so the average energy remains steady at a mean value. The term $-\sum_{i<j} \nabla U(r_{ij})$ is the force comprised of interparticle interactions. Also,

$$\boldsymbol{F}_{ext} = \boldsymbol{F}_E + \boldsymbol{F}_B \qquad (2.2)$$

is the force comprised of the external force fields. Here, $\boldsymbol{F}_E$ is the space-independent external electric force acting on the particles pointing in the Y direction, and is

modelled as

$$F_E(t) = \hat{y} E_0 \cos(\omega t), \tag{2.3}$$

where E_0 is the strength or amplitude of the external electric field, ω is the frequency of the external electric field (with $\omega \equiv 0$ leading to the constant-field case) and $\hat{y}$ is the unit vector along Y direction. Force

$$F_B = \frac{Q_{A,B}B}{m_i c} \dot{r}_i \times \hat{e}_z \tag{2.4}$$

is the force due to the external magnetic field applied along the Z direction (i.e. out of the simulation box), where c is the speed of light (Baruah *et al.* 2021). The strength of the magnetic field B is given by $\beta = \omega_c/\omega_{pd} \propto B$ (with $\beta \equiv 0$ leading to the case of the system in the absence of magnetic field), where $\omega_c = Q_{A,B}B/m_i c$ represents the cyclotron frequency and $\omega_{pd} = [2Q_{A,B}^2/4\pi\epsilon_0 a^3 m]^{1/2}$ is the plasma frequency. Parameter a is the Wigner–Seitz radius, ϵ_0 is the permittivity of free space and $Q_{A,B}$ is the charge of particle A (B). The trajectories of the PIP are determined by all the factors mentioned above in (2.1)

The interaction potential reads as

$$U(r_{ij}) = \left(\frac{Q_A Q_B}{4\pi\epsilon_0 r_{ij}} \right) \exp\left(-\kappa \left(\frac{r_{ij}}{a} - 1 \right) \right), \tag{2.5}$$

where r_{ij} is the distance between ith and jth pair and $Q_{A,B}$ is the charge of particle A (B), such that $Q_A Q_B = -1$ and $Q_A Q_A = Q_B Q_B = +1$. Here, the length, time, energy, density and electric field are normalized respectively by: a, ω_{pd}^{-1}, $k_B T$, a^2 and $Q/4\pi\epsilon_0 a^2$. In these units, the strength of the interaction potential is defined as Γ, where $\Gamma = Q_{A,B}^2/4\pi\epsilon_0 a k_B T$, in which $k_B T$ denotes the thermal energy.

For this study, the stochastic Langevin normalized equations for the particle trajectories $r_i(t)$ ($i = 1, \ldots, N$) read as

$$\frac{d^2 r_i}{dt^2} = -\gamma \frac{dr_i}{dt} + \sum_{i<j} \frac{\Gamma}{r_{ij}} \left(\kappa + \frac{1}{r_{ij}} \right) \exp[-\kappa(r_{ij} - 1)] + F_{ext}(t) + F_i^{(R)}(t). \tag{2.6}$$

3. Simulation procedure

Extensive Langevin dynamics simulations using OpenMP parallel program are carried out to analyse the effect of obstacle and geometric aspect ratio on lane formation dynamics in the 2-D PIP system. Simulations are performed using N particles in a rectangular simulation cell having sides L_x, L_y, which are so chosen that the geometric aspect ratio A varies as $A = L_x/L_y = 2.0, 3.0, 4.0, 5.0, 6.0, 7.0, 8.0, 9.0, 10.0, 20.0, 30.0, 40.0$, at fixed density ρ. In the process of deciding the appropriate number of particles N we have performed a series of runs at fixed density ρ, such that the finite size effects tend to become negligible. As already mentioned above, a 2-D small square box having dimensions $(l_x \times l_y)$ is created inside the main simulation chamber representing an obstacle. Along all sides of this small box SRBCs are applied. However, periodic boundary conditions are applied along the boundaries of the main simulation chamber. After equilibration with the desired temperature Γ^{-1}, using the Langevin equation, a force due to the external electric field F_E is applied to the particles. Here, the external magnetic field is applied from the beginning of the simulation. The lane or structure order parameter (defined later) is evaluated for the electric field strength value $E_0 > E_c$ (E_c denotes the critical value

of the field strength). Each particle is assigned an initial velocity which is random in magnitude and direction such that the average kinetic energy corresponds to the chosen temperature. The particles move according to the Langevin equations of motion. Here, the equations of motion are solved using the velocity-Verlet method with a sufficiently small time step $\Delta t = 0.003$. The simulation is done in the following steps (for a typical run, say, at $\Gamma = 2.5$, $\kappa = 0.0001$, $\rho = 1.0$). For constant and oscillatory applied electric fields, considering cases both with and without external magnetic field, typically $2 \times 10^6 \Delta t$ steps are simulated which corresponds to a simulation time of $t\omega_{pd} = 6000$ with $\Delta t = 3 \times 10^{-3}$. After equilibration at a desired thermal energy using the Langevin equation, the external force field is applied to the particles at a time $t = 2 \times 10^5 \Delta t$ steps. Data collection is obtained for the last $2 \times 10^5 \Delta t$ steps after the system has reached a far-from-equilibrium quasi-steady state.

3.1. *Order parameter (instantaneous)*

To quantify the lane formation observed in our system, following Ikeda & Kim (2017); Sarma *et al.* (2020), we introduce an order parameter ϕ as follows. First, the simulation system is divided into n_{div} number of identical rectangular strips along the driven direction (i.e. along $\hat{y}$). Thus, the width of each strip along the x direction is given by $l_{div} = L/n_{div}$. The order parameter for lane formation, say, in the kth strip is defined as

$$\phi_k = \frac{n_k^+ - n_k^-}{n_k^+ + n_k^-}, \tag{3.1}$$

where $n_k^{\pm}$ represents the number of '$\pm$' species in the kth rectangular strip. The order parameter ϕ for the total system is then defined as

$$\phi = \left\langle \frac{1}{n_{div}} \sum_{k=1}^{n_{div}} |\phi_k| \right\rangle, \tag{3.2}$$

where the brackets denote a time average. By definition, ϕ changes from 0 to 1. For randomly mixed configuration, ϕ is close to zero, while it approaches unity as the system evolves the laning order.

3.2. *Cumulative order parameter (ϕ')*

Cumulative order parameter (ϕ') calculates the cumulative total (or running sum) of a set of input values of order parameter ($\phi - \phi_c$); it is also time-averaged. It is defined by

$$\phi'(t') = \frac{1}{t'} \int_{t_{on}}^{t_{run}} (\phi - \phi_c) \, dt'. \tag{3.3}$$

Here, t_{on} is the simulation time when the external electric field is applied to the system and ϕ' is calculated until time t_{run}, where t_{run} denotes the simulation time when the external electric field is turned off. As already mentioned above, $\phi = \phi_c = 0.5$ is the critical value of order parameter, where the lane formation of the PIP system just started, and $t' = (t_{on} + idt') - t_{on}$, where $i = 1, 2, 3, \ldots$. Here, we divide the order parameter plot into identical rectangular strips. The right-hand side of (3.3) represents the exact area under the graph of $(\phi - 0.5)$ between t_{on} and t_{run}. Intuitively, it is the infinite sum of all rectangles with height $(\phi(t) - 0.5)$ and width dt', and we are summing over all t in the interval $[t_{on}, t_{run}]$; it is also the time-averaged. This method helps in quantifying the 'order' of our PIP system.

3.3. *Occurrence distribution function of ϕ ($f(\phi)$)*

This diagnostic technique is used to evaluate the occurrence distribution function of the instantaneous order parameter (ϕ) during the whole simulation run. In order to do so, a counter is set which counts the ϕ value at every interval of time and records which range of ϕ values occurred how many times. Thus, this technique produces a distribution function of ϕ. The ϕ value occurring the maximum number of times indicates that the system remained at that particular value for the majority of the simulation run. Thus, this helps us in further clarifying the ordering in the PIP system. The curve obtained following the method described above may be divided into two parts: in one part $\phi < (\phi_c = 0.5)$ values are plotted and in the other part $\phi \geq (\phi_c = 0.5)$ values are plotted. By observing the area under the curve obtained in these ways one can distinguish whether our PIP system is in lane formation phase or in disordered phase.

3.4. *The Y-averaged charge profile $\bar{Q}(x, t)$*

A charge profile plot is a graphical data analysis technique for examining the relative behaviour of all charged (PIP) particles in a multivariate dataset. The measurement of charge distribution is crucial in the PIP system to ensure the geometric structures of the lane such as the lane number and lane width. This diagnostics technique consists of a sequence of vertical spikes with each spike representing a different variable (here, '$\pm$' PIP particle species). An individual charge profile plot examines the behaviour of all such species. An interconnecting line cutting across each spike at the 'data length' gives the charge profile plot.

To implement this technique the whole simulation chamber is virtually divided into n_{div} number of small identical rectangular strips (along the Y direction, which is the driven direction) of thickness l_{div} along the X direction. The total charge in each individual rectangular strip is calculated by adding the charges of each PIP particle in the strip. Averaging this quantity in each strip over the total simulation time step gives the Y-averaged charge profile $\bar{Q}(x, t)$. In this Y-averaged charge profile plot, $\bar{Q} > 0$ indicates the presence of a lane composed of positively charged PIP particles, while $\bar{Q} < 0$ indicates the presence of a lane consisting of negatively charged PIP particles. The case $\bar{Q} = 0$ acts as a separation boundary for lanes of positively and negatively charged particles, where mixing of lanes formed by oppositely charged PIP particles takes place and as a result of which the peak height may reduce and in some cases make the $\bar{Q}$ value approximately zero. On the other hand, the lane width can be predicted by observing the thickness of the spikes. Thus, this diagnostic technique is very useful in predicting lane numbers and their thickness in small time domain.

Here, we focus on a 2-D PIP system and explore the effect of geometric aspect ratio and obstacle on the lane formation dynamics in both the presence and absence of an external magnetic field. Further, to identify non-equilibrium phase transition, time variations of instantaneous order parameter (ϕ), cumulative order parameter (ϕ') and $f(\phi)$ are studied; however, to study the geometric structure of the lanes, Y-averaged charge profile $\bar{Q}(x, t)$ is calculated. In the entire work these diagnostic techniques are used.

4. Results and discussion

In this paper, we perform our study to see the effect of an obstacle and geometric aspect ratio on lane formation dynamics in the PIP system in both the presence and absence of an external magnetic field. Both constant ($\omega = 0$) and time-varying ($\omega \neq 0$) external electric fields are applied to drive the system. The aspect ratio is a fundamental quantity that denotes proportional ratio between the individual system sizes. We find that the lane

formation does not depend on either L_x or L_y individually (L_x, L_y represent system lengths); rather the aspect ratio L_y/L_x appears to be an important quantity. We have systematically examined this lane formation dynamics with different aspect ratio values varying from $L_y/L_x = 1$ to $L_y/L_x = 40$ (although results for only a few values of L_y/L_x are shown). Additionally, we have also performed a comparative study of the results obtained in both the presence and absence of an external magnetic field to see the effect of geometric aspect ratio and obstacle on lane formation dynamics in the PIP system, the details of which are discussed in § 4.3. This work primarily focuses on the determination of the parameter regime of existence of lane structures in the PIP system in the zero screening limit where the the obstacle and simulation chamber with varying aspect ratio play an important role.

4.1. *Lane formation in the presence of constant ($\omega = 0$) electric field*

In this subsection, we report on comprehensive simulation studies of lane formation in the PIP system, carried out in the presence of a constant external electric field. Here, we focus on the influence of the obstacle and geometric aspect ratio on the lane dynamics.

4.1.1. *Without obstacle*

In figure 2 typical simulation snapshots associated with a situation are shown where the effect of the aspect ratio on lane formation dynamics is studied using an asymmetric simulation chamber. The simulation snapshots are plotted at the end of every simulation run, i.e. $t\omega_{pd} = 6000$, showing the instantaneous particle positions for aspect ratio values $L_y/L_x = 1, 3, 7, 10, 20$ and 30. This part of the study is performed in the absence of the obstacle. It is evident from our earlier work (Sarma *et al.* 2020) that an external electric field greater than some critical value of the field strength E_c is required for the formation of lanes in a PIP system. The critical value of the electric field strength E_c is determined at the electric field strength value where generation of lane formation just started and the corresponding value of the order parameter is recorded as $\phi = 0.5$ (Sarma *et al.* 2020; Baruah *et al.* 2021) for the simulation runs with increasing field strength and this value of order parameter is considered as the critical value (ϕ_c). Thus, for this study, electric field strength in all simulation runs is taken to be $E_0 = 150$ which is much greater than E_c for the simulation runs under study. The other parameters used are $\Gamma = 2.5$, $\kappa = 0.0001$ and $\rho = 1.0$. From the figure, one clearly sees lane formation parallel to the external electric field. However, it is observed that the geometric structure of the lanes, i.e. lane width and lane numbers, is affected by the aspect ratio values. This can also be realized from figure 3, where Y-averaged charge profile $\bar{Q}(x, t)$ is plotted corresponding to the instantaneous particle snapshots recorded at $t\omega_{pd} = 6000$ and shown in figure 2. It is worth noting that the crest and trough in figure 3, corresponding to different aspect ratio values, occur precisely for the case exhibited in figure 2, i.e. the system is arranged into a lane structure with a well-defined symmetry.

Figure 3 shows the charge profiles normal to the walls for the aforementioned channel widths. It is evident that a strong dependence exists between the system structure (number of lanes) and simulation chamber width. It is also evident that there is a clear accumulation of particles at walls, as indicated by the sharp peaks (see figure 3). On the other hand, from figure 2 it is seen that for lower aspect ratio value, four lanes per species of particle appear, which further decreases to three (sometimes two) lanes per species of particle for mid-range of aspect ratio values. Further, at higher values of the aspect ratio, the lanes of individual species have a tendency to merge and form two lanes, one for each species of particles. Our observation is also supported by the Y-averaged charge profile $\bar{Q}(x, t)$ versus L_x (see figure 3) plotted for different aspect ratio values $A = L_y/L_x = 1, 3, 7, 10, 20$ and 30 in the absence of the obstacle, where $\bar{Q} > 0$ indicates the presence of a lane composed of
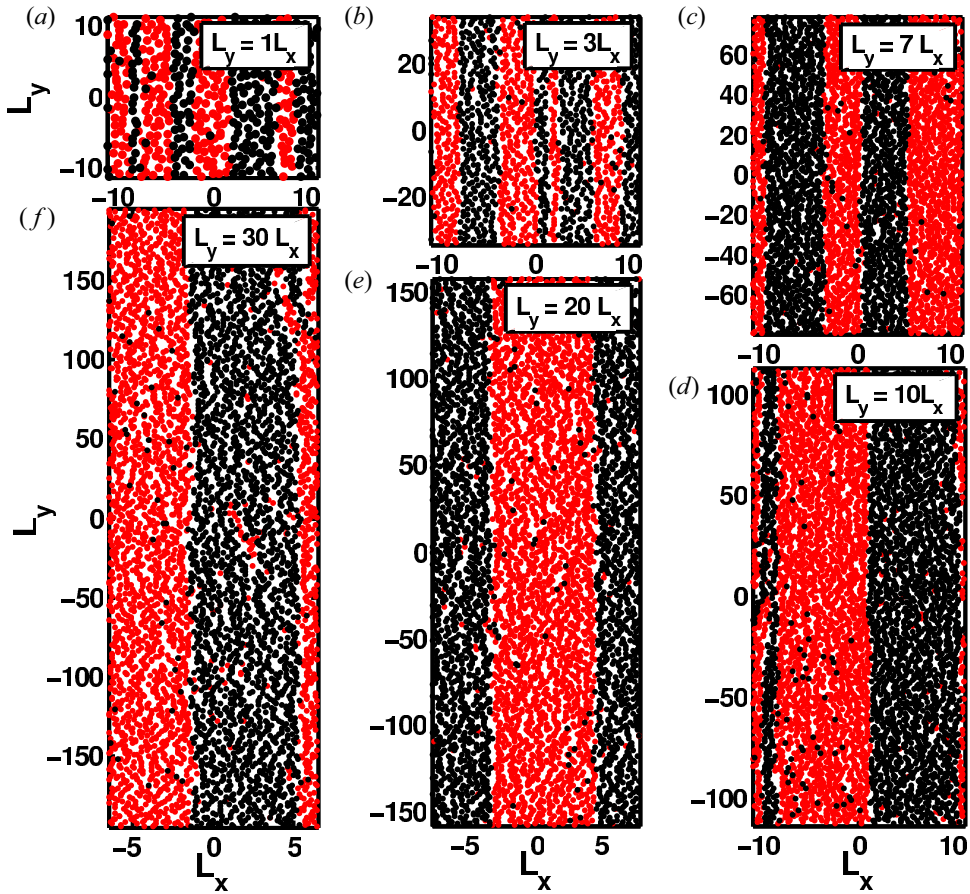
FIGURE 2. Typical simulation snapshots of the 2-D PIP system with constant external electric field ($\omega = 0$) in the absence of an obstacle are plotted by taking aspect ratio values $L_y = L_x$, $L_y = 3L_x$, $L_y = 7L_x$, $L_y = 10L_x$, $L_y = 20L_x$ and $L_y = 30L_x$. The snapshots are recorded at time $t\omega_{pd} = 6000$. The other parameters used are $\Gamma = 2.5$, $E_0 = 150$. Here, the external electric force F_E is applied along the Y direction.

positively charged PIP particles, while $\bar{Q} < 0$ indicates the presence of a lane consisting of negatively charged PIP particles. Figure 3 also shows that the Y-axis values increase for larger values of aspect ratio. At higher aspect ratios, the length of the simulation chamber increases along the $\hat{Y}$ direction which results in a longer strip at higher aspect ratio values. This longer strip can accommodate a greater number of particles and thus gives a higher value of total charge $\bar{Q}$ along the Y axis. Hence, $\bar{Q}$ is expected to increase for higher aspect ratio values. The observed tendency of merging of lanes with increasing aspect ratio values could be the tendency of the system to increase the flow efficiency. Figure 2 also indicates that the width of the lanes increases gradually with increasing aspect ratio values. In the snapshots, this width of the lanes involves several particle layers, which increases with increasing aspect ratio value and is comparable with the size of the simulation box. The spike width of the Y-averaged charge profile $\bar{Q}$ plot (figure 3) also supports the above-mentioned observation. This implies that lane formation is a macro-phase separation. It may be conjectured that when a two-lane state is formed from
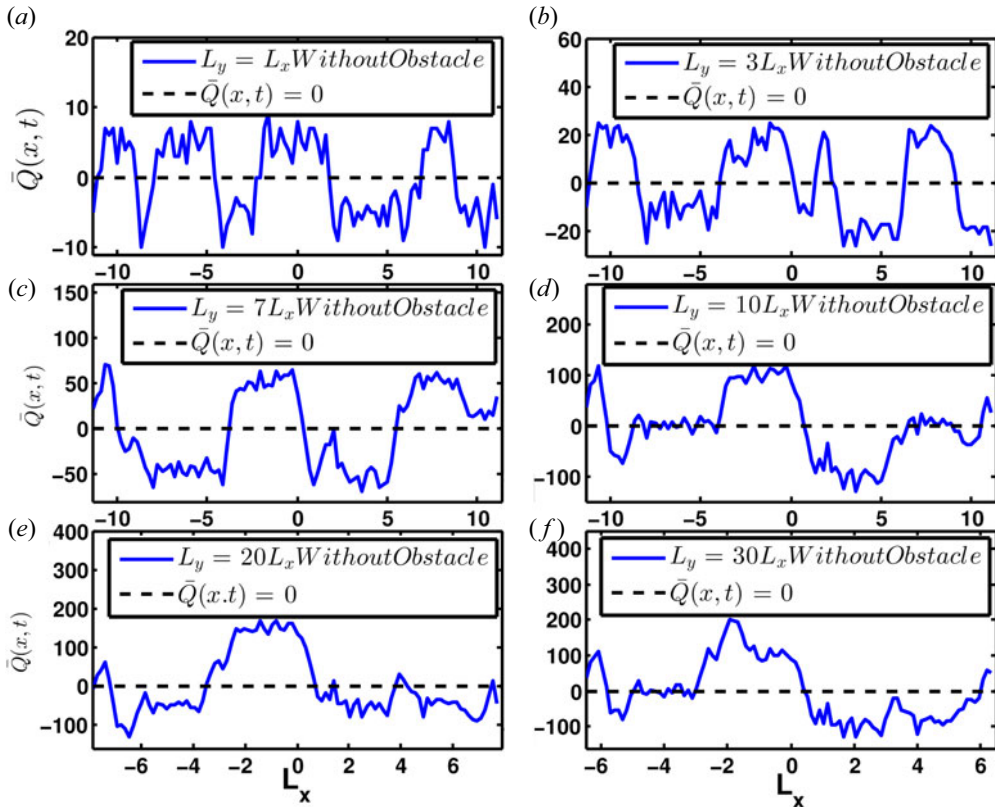
FIGURE 3. The Y-averaged charge profile $\bar{Q}(x, t)$ is plotted corresponding to the instantaneous particle snapshots recorded at $t\omega_{pd} = 6000$ as shown in figure 2. The $\bar{Q}(x, t)$ profile is plotted of the 2-D PIP system for constant external electric field ($\omega = 0$) in the absence of the obstacle taking aspect ratio values $L_y/L_x = 1, 3, 7, 10, 20$ and 30. The other parameters used are $\Gamma = 2.5$, $E_0 = 150$.

the disordered initial configuration for higher aspect ratio value, the number of collisions between different PIP species increases with the system size. To reduce such energy loss due to collisions, the lane should be split to increase the lane width.

In figure 4, the order parameter ϕ is plotted against $t\omega_{pd}$ for aspect ratio values $L_y/L_x = 1, 3, 7, 10, 20$ and 30. The figure indicates that the fluctuations in order parameter values increase with increasing aspect ratio. With increasing aspect ratio the lanes have a longer distance to travel along the y axis and friction at the interface between oppositely driven PIP particles takes place. As a consequence of that, as shown in figure 5 with the help of circles, the older lanes are broken down and new lanes are formed very often, which tends to disturb the stability of the lanes, and this is very evident from the fluctuations in time variation of the order parameter (ϕ) plot as shown in figure 4.

A typical result for the occurrence distribution function of ϕ (or $f(\phi)$) as a function of instantaneous ϕ is shown for the 2-D PIP system and a constant external electric field ($\omega = 0$) in figure 6. These results are obtained in the absence of the obstacle and for different geometric aspect ratio values $L_y = L_x$, $L_y = 3L_x$, $L_y = 7L_x$, $L_y = 10L_x$, $L_y = 20L_x$ and $L_y = 30L_x$. The other parameters used are $\Gamma = 2.5$ and $E_0 = 150$. As already mentioned above, here the location of the phase transition is estimated from the
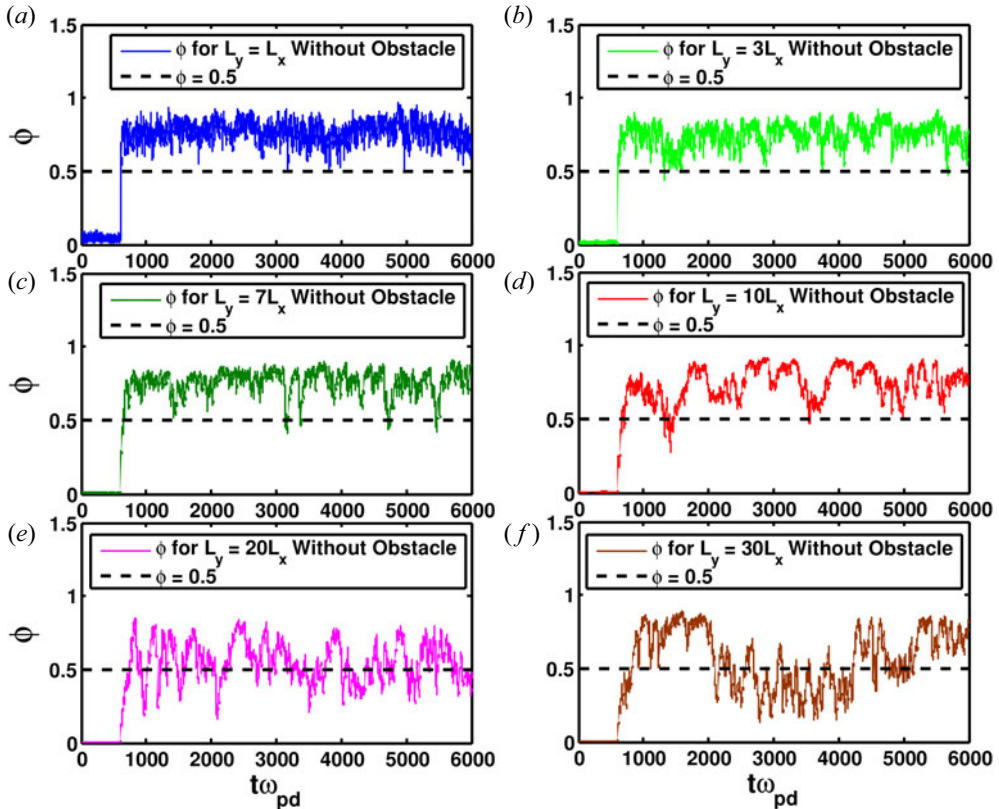
FIGURE 4. Order parameter ϕ versus $t\omega_{pd}$ of the 2-D PIP system for constant external electric field ($\omega = 0$) in the absence of the obstacle is plotted by taking aspect ratio values $L_y = L_x$, $L_y = 3L_x$, $L_y = 7L_x$, $L_y = 10L_x$, $L_y = 20L_x$ and $L_y = 30L_x$. The other parameters used are $\Gamma = 2.5$, $E_0 = 150$.

behaviour of the order parameter. The location of phase transition is obtained by setting $\phi \simeq 0.5$ for a set of runs with different aspect ratio. In figure 6 for aspect ratio value $L_y/L_x = 1$ the whole curve exists in the domain where $\phi > 0.5$, indicating that the system is in a complete lane state. With increasing value of the aspect ratio the $f(\phi)$ curve widens and shifts gradually towards $\phi \leq 0.5$ domain. On further increasing the aspect ratio value to $L_y/L_x = 20$, almost half of the area under the $f(\phi)$ curve shifts towards $\phi \leq 0.5$ domain, where the system enters in partially lane mixing phase. However, on further increasing the aspect ratio value, the lane mixing tendency also increases in our PIP system as can be understood from the plot for $L_y = 30L_x$ of figure 6. Our observation is further verified by figure 7, where the occurrence distribution function $f(\phi)$ is calculated for different geometric aspect ratio values, namely $L_y = L_x$, $L_y = 7L_x$, $L_y = 10L_x$ and $L_y = 20L_x$, after turning on the external electric field at $t\omega_{pd} = 600$ simulation time step. The area under each curve is recorded for various simulation time zones. The whole observation is performed during $t\omega_{pd} = 600$ (i.e. when the external electric field is just turned on) to $t\omega_{pd} = 6000$ time steps (i.e. when the electric field is just turned off at the last simulation time step). This time interval is divided into four equal time zones and measurement of the number of occurrences of ϕ as a function of ϕ (instantaneous) corresponding to each time zone is recorded and plotted separately as shown in figure 7. The figure indicates
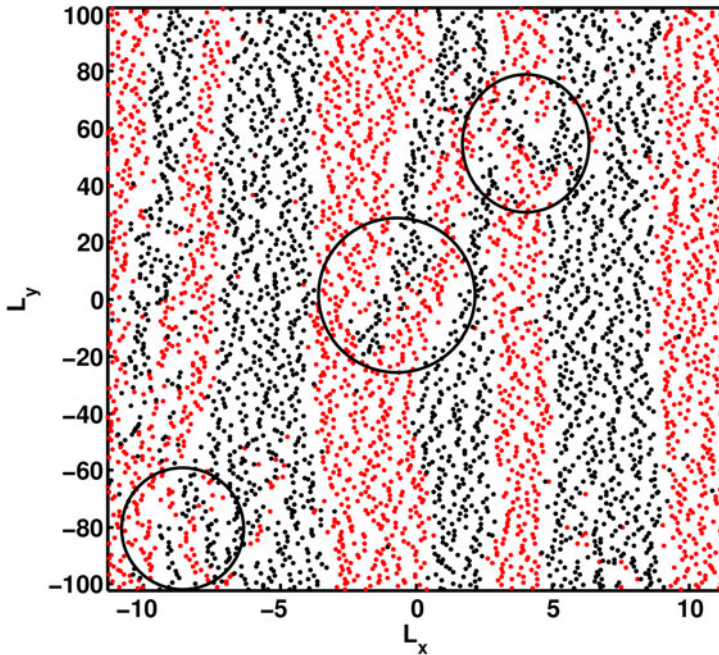
FIGURE 5. Typical simulation snapshot of instantaneous particle positions of the 2-D PIP system without the obstacle and in the presence of constant ($\omega = 0$) external electric field is plotted. The snapshot shows the breaking of lanes (as indicated by the three circles) due to the friction at the interface between oppositely driven PIP particles. Aspect ratio value used is $L_y = 9L_x$. The other parameters used are $E_0 = 150$, $\Gamma = 2.5$, $\kappa = 0.0001$, $\rho = 1.0$.

that for $L_y = L_x$ (see figure 7a) in all four time zones the area under the curve remains in the domain where $\phi > 0.5$, i.e. the system is in a lane state for the whole simulation time. A similar kind of behaviour with a slight spreading of the area under the curve is observed with increasing aspect ratio values to $A = L_y/L_x = 7$ and 10. However, on further increasing the aspect ratio value to $A = L_y/L_x = 20$, a shifting of almost half of the area under the curve towards $\phi \leq 0.5$ region is observed, which indicates the mixing of lanes in the PIP system. For the rest of the work we used the above procedure to distinguish whether our PIP system is in ordered lane state, lane mixing state or disordered state for all other values of geometric aspect ratio, in both the presence and absence of the obstacle.

To identify the region of phase transition, we now focus on the time variation of cumulative order parameter (ϕ') plotted for constant external electric field ($\omega = 0$) in the absence of the obstacle (see figure 8). For this, the aspect ratio values used are $L_y = L_x$, $L_y = 3L_x$, $L_y = 7L_x$, $L_y = 10L_x$, $L_y = 20L_x$ and $L_y = 30L_x$. The other parameters used are $\Gamma = 2.5$ and $E_0 = 150$. Figure 8 indicates that for lower values of aspect ratio, i.e $L_y/L_x < 20$, the PIP system remains in lane state throughout the simulation time. For larger aspect ratio values, i.e. $L_y/L_x \geq 20$, the PIP particles get comparatively more chance to interact with oppositely driven particles. As a result, the particles are likely entangled into another lane, which tends to disturb the stability of the lanes and as a result of which the cumulative order parameter ϕ' curve shifts towards $\phi' = 0$. Our result is consistent with that predicted by the time variation of ϕ (see figure 4) and also the occurrence distribution function $f(\phi)$ plot as shown in figure 6.
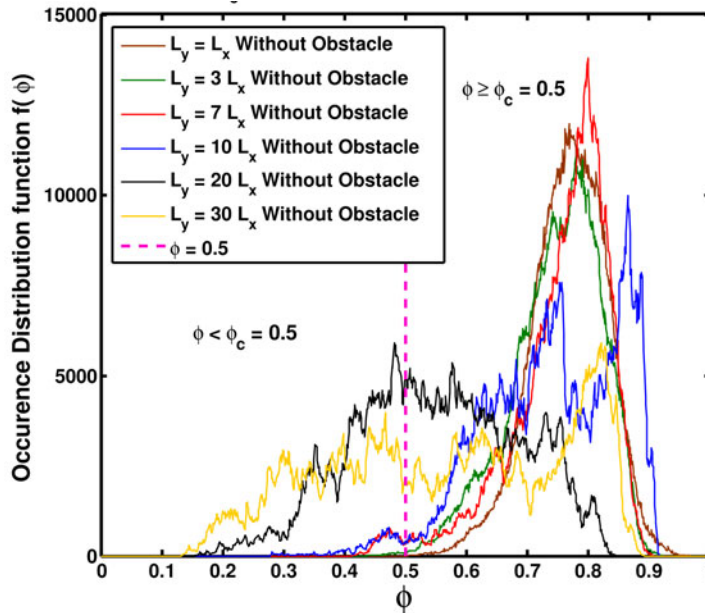
FIGURE 6. Occurrence distribution function of ϕ (or $f(\phi)$) versus instantaneous order parameter ϕ of the 2-D PIP system for constant external electric field ($\omega = 0$) in the absence of the obstacle is plotted by taking aspect ratio values $L_y = L_x$, $L_y = 3L_x$, $L_y = 7L_x$, $L_y = 10L_x$, $L_y = 20L_x$ and $L_y = 30L_x$. The other parameters used are $\Gamma = 2.5$, $E_0 = 150$. This figure helps in clarifying the ordering in the PIP system.

4.1.2. *With obstacle*

In this subsection, the lane formation dynamics of the PIP system is studied in the presence of an obstacle. For this, the obstacle is applied having dimensions $l_x \times l_y$ at the centre of the simulation box. Here, all the simulations are carried out for $l_x = l_y = 3.78$. In particular, we have examined the effect of the obstacle on lane formation using a simulation chamber having various geometric aspect ratio values.

In figure 9(*a*), the instantaneous positions of the particles are plotted as recorded at the end of every simulation run (i.e. at $t\omega_{pd} = 6000$ time step) for an external electric field having strength $E_0 = 150$, frequency $\omega = 0$, $\Gamma = 2.5$ and with aspect ratio values $L_y = L_x$, $L_y = 3L_x$, $L_y = 7L_x$, $L_y = 10L_x$, $L_y = 20L_x$ and $L_y = 30L_x$. From this figure it is observed that with the introduction of the obstacle the merging tendency of lanes increases even at lower values of the aspect ratio (see figure 9*a*) as compared to that in the absence of the obstacle (see figure 2). The presence of the obstacle may improve the flow rate by merging all the individual groups of particles of the same species and resulting in two separate lanes, one for each species of the particles. However, for the same set of parameters under study, this property is not observed in the absence of the obstacle (see figure 2) even at lower values of aspect ratio. In the present case, the presence of the obstacle is the main contribution to the merging of lanes and their stability. Figure 9(*a*) also shows that the PIP system loses stability of the lane structures with increasing geometric aspect ratio values. In the presence of the obstacle the system enters into a partially mixed phase with aspect ratio value $L_y/L_x \geq 9$, where $L_y/L_x = 9$ acts as a transition point. This transition of the lane state to partially mixed state occurs even in the presence of an external electric field with strength $E_0 \geq E_c$.
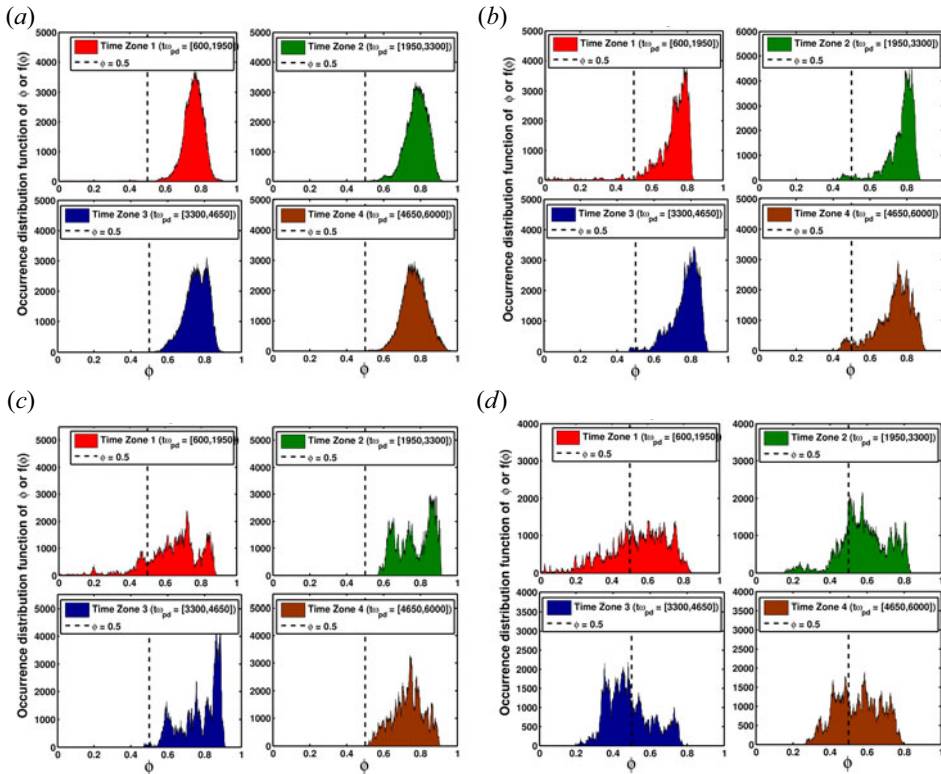
FIGURE 7. Occurrence distribution function of ϕ ($f(\phi)$) is calculated for different geometric aspect ratio values (*a*) $L_y = L_x$, (*b*) $L_y = 7L_x$, (*c*) $L_y = 10L_x$ and (*d*) $L_y = 20L_x$, after turning on the external electric field at $t\omega_{pd} = 600$ simulation time step. The area under each curve is recorded for various simulation time zones of the 2-D PIP system for constant external electric field ($\omega = 0$) in the absence of the obstacle. The other parameters used are $\Gamma = 2.5$, $E_0 = 150$.

Our result is supported by the corresponding lane formation order parameter ϕ versus $t\omega_{pd}$ plot, as shown in figure 9(*b*), and time variation of cumulative order parameter ϕ', as shown in figure 10. The other parameters used are $E_0 = 150$ and $\Gamma = 2.5$, and with aspect ratio values $L_y = L_x$, $L_y = 3L_x$, $L_y = 7L_x$, $L_y = 10L_x$, $L_y = 20L_x$ and $L_y = 30L_x$. Figure 9(*b*) shows that in the presence of the obstacle the order parameter struggles to cross the structure formation constraint of $\phi = \phi_c = 0.5$ at lower aspect ratio value. However, at moderate to higher value of the aspect ratio the curve gradually approaches the $\phi = 0.5$ limit and decreases beyond the critical value of $\phi_c = 0.5$ at some points of simulation. Additionally, the fluctuation of the order parameter plots also increases, which indicates that the system has a tendency to transition from an ordered lane state to a disordered lane mixing state. On the other hand, in figure 10 the time variation of cumulative order parameter ϕ' is measured to obtain insight into how often the instantaneous order parameter ϕ is below $\phi = 0.5$, so that it may be helpful in describing a situation in which the lane mixing phenomenon is involved. Our observation shows that figure 10 supports the argument of the critical value of aspect ratio being $L_y/L_x = 9$ in the presence of an obstacle in our PIP system. For aspect ratio value $L_y/L_x < 9$, the system shows a lane state and for higher aspect ratio value the curve almost remains under the $\phi = 0.5$ barrier throughout the simulation time.
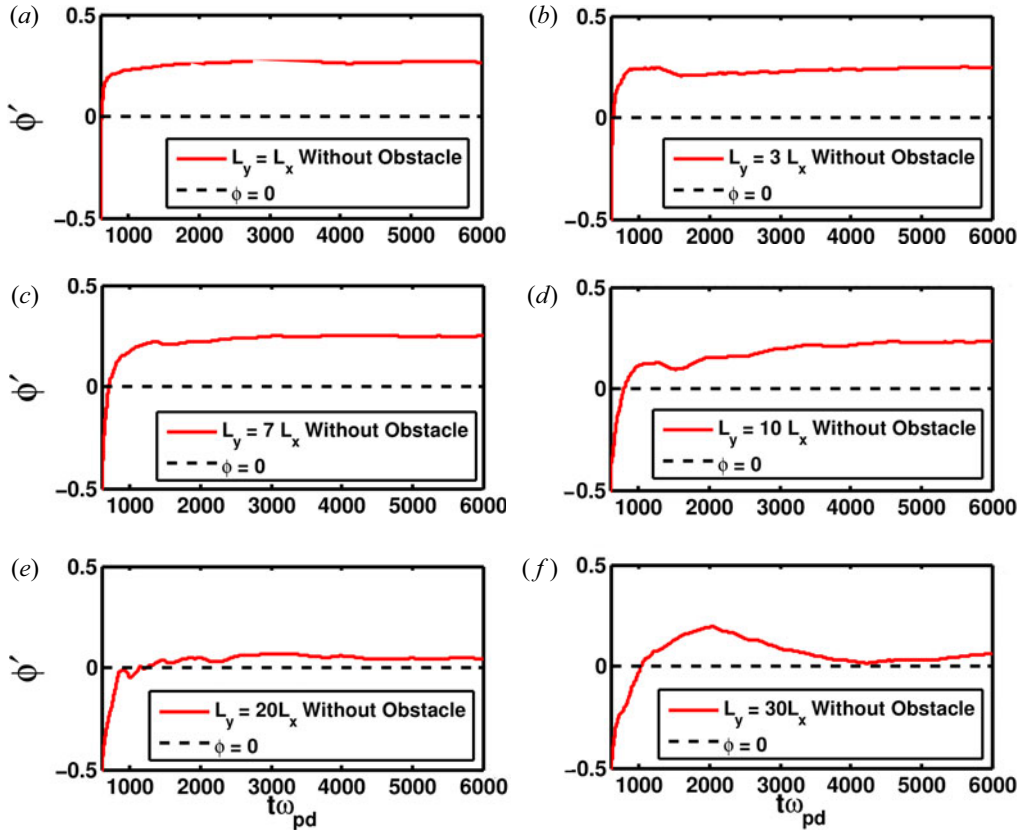
FIGURE 8. Cumulative order parameter ϕ' versus $t\omega_{pd}$ plots of the 2-D PIP system for constant external electric field ($\omega = 0$) in the absence of the obstacle. The aspect ratio values used are (a) $L_y = L_x$, (b) $L_y = 3L_x$, (c) $L_y = 7L_x$, (d) $L_y = 10L_x$, (e) $L_y = 20L_x$ and (f) $L_y = 30L_x$. The other parameters used are $\Gamma = 2.5$, $E_0 = 150$.

In figure 11 the occurrence distribution function $f(\phi)$ as a function of instantaneous ϕ in the presence of the obstacle is plotted for aspect ratio values $A = L_y/L_x = 1, 3, 7, 10, 20$ and 30, taking $\Gamma = 2.5$ and $E_0 = 150$. The figure indicates that for lower values of A the whole curve remains in the domain $\phi \geq 0.5$, indicating a homogeneous lane state. For the medium aspect ratio values the distribution curve widens and shifts gradually more and more towards the left-hand side indicating a reduction in ordering in the system. Further, at higher values of aspect ratios for $A = 20$ and 30 this widened curve shifts to a domain of $\phi < 0.5$, indicating a state of lane mixing or a partially disordered state.

The occurrence distribution function of $f(\phi)$ for a few such distributions as indicated in figure 11 are shown in figure 12, for aspect ratio values $A = 1, 7, 10$ and 20. Time zone analysis is performed during the simulation time $t\omega_{pd} = 600$ (when the electric field is just turned on) to 6000 (when the electric field is just turned off), by dividing the whole area under the curve into four equal time zones as shown in figure 12 for the same parameters used in the case of figure 11. Figure 12(a) indicates that for $A = 1$ the system is in lane state, as the area under the $f(\phi)$ curve remains in $\phi > 0.5$ domain in all four time zones. For $A = 7$, despite the widening of the $f(\phi)$ curve due to fluctuations, the system attains an ordered state over time; however, it takes some time to attain the ordered state, i.e. in the fourth time zone (i.e. at the end of the simulation) a large majority of the distribution
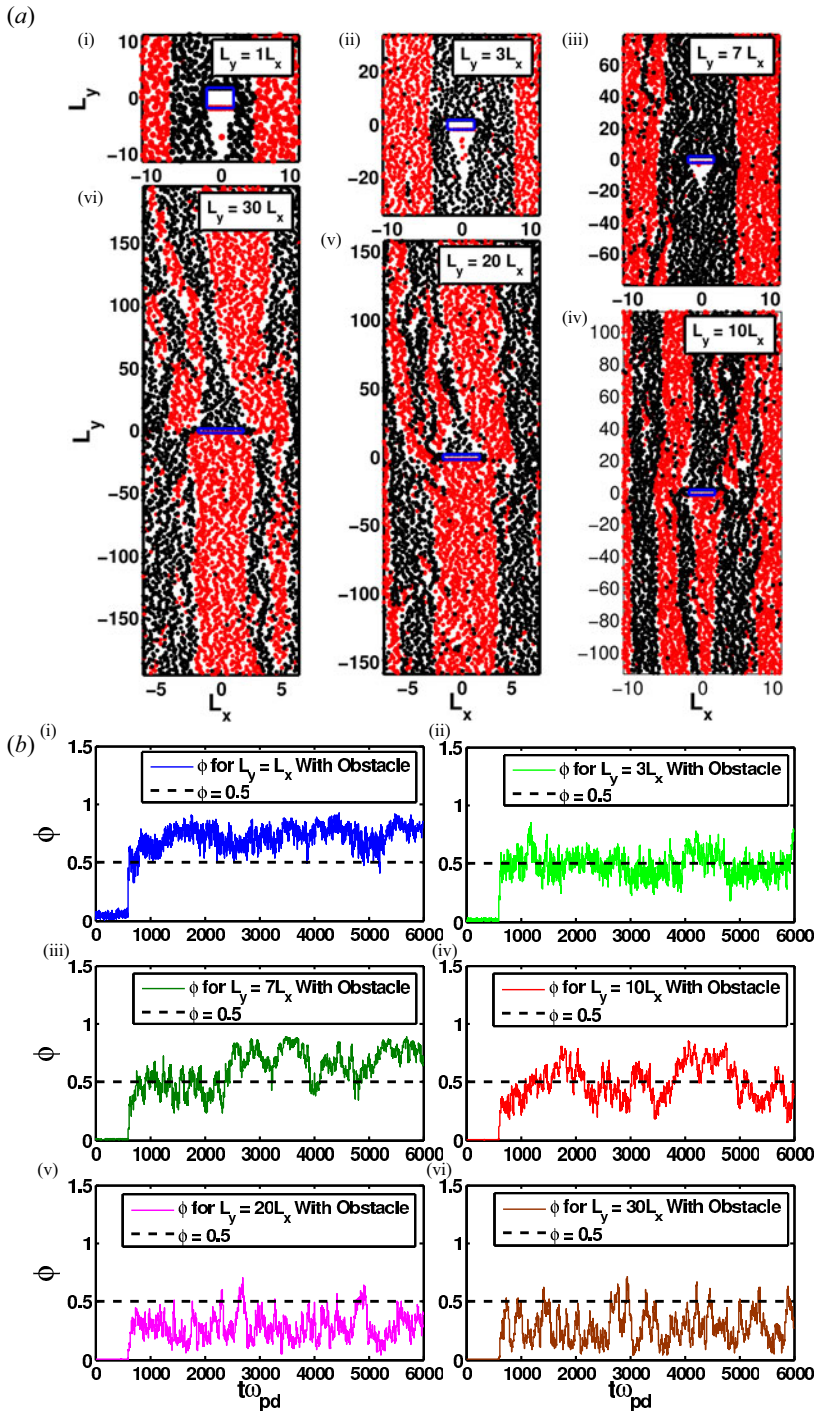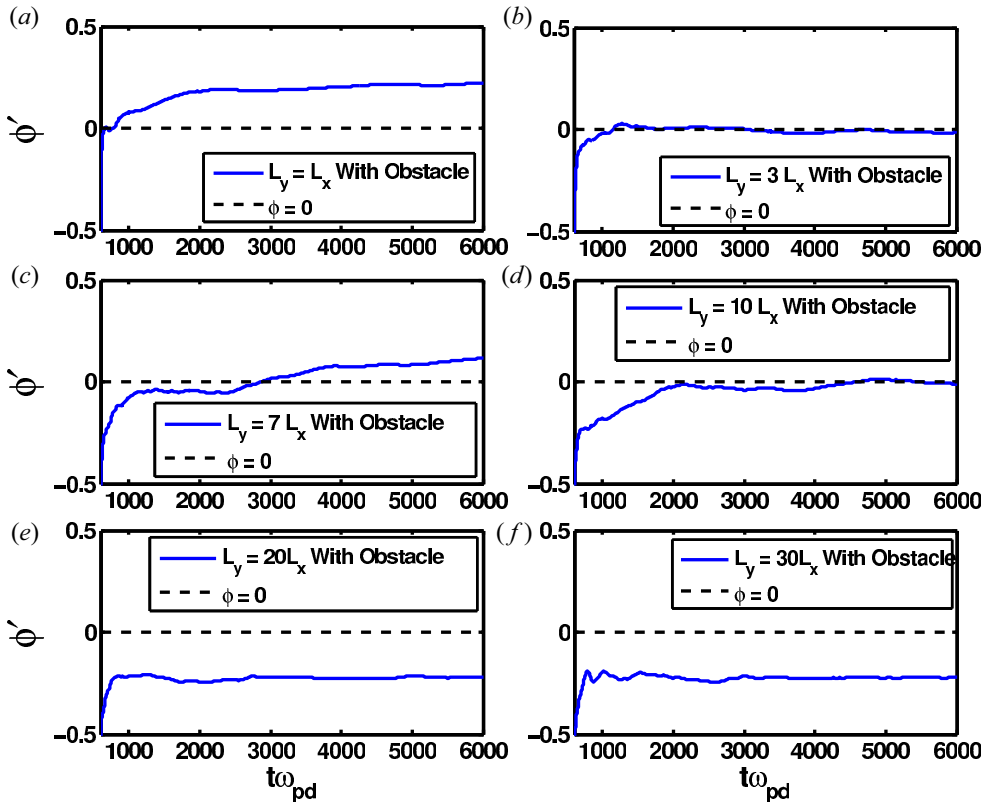
FIGURE 9. (*a*) Typical simulation snapshots of the 2-D PIP system with constant external electric field ($\omega = 0$) in the presence of the obstacle are plotted by taking aspect ratio values (i) $L_y = L_x$, (ii) $L_y = 3L_x$, (iii) $L_y = 7L_x$, (iv) $L_y = 10L_x$, (v) $L_y = 20L_x$ and (vi) $L_y = 30L_x$. The snapshots are recorded at time $t\omega_{pd} = 6000$. (*b*) The corresponding order parameter ϕ versus $t\omega_{pd}$ plots. The other parameters used are $\Gamma = 2.5$, $E_0 = 150$. Here, the external electric force F_E is applied along the Y direction.

FIGURE 10. Cumulative order parameter ϕ' versus $t\omega_{pd}$ plots of the 2-D PIP system for constant external electric field ($\omega = 0$) in the presence of the obstacle. The aspect ratio values used are (a) $L_y = L_x$, (b) $L_y = 3L_x$, (c) $L_y = 7L_x$, (d) $L_y = 10L_x$, (e) $L_y = 20L_x$ and (f) $L_y = 30L_x$. The other parameters used are $\Gamma = 2.5$, $E_0 = 150$.

curve remains in the ordered domain of $\phi \geq 0.5$ (see figure 12b). On further increasing the aspect ratio value to $A = 20$ the PIP system gradually transitions to a partially disordered state as indicated in figure 12(c). While figure 12(d) indicates along with the inclusion of fluctuations the system can also be in the domain of $\phi < 0.5$ for the majority of the time, indicating a lane mixing or disordered phase. A higher aspect ratio thus tends to direct the system towards a lane mixing state despite being acted upon by an external electric field $E_0 > E_c$.

To investigate the effect of the friction coefficient (γ) on the lane formation dynamics, an extensive simulation study by varying the value of γ as $\gamma = 7, 10$ and 20 has been performed in the presence of both constant and time-varying electric fields in both the absence and presence of the obstacle (corresponding results except the constant electric field with obstacle case are not mentioned in this study). In figure 13 the instantaneous positions of the particles are plotted as recorded at the end of every simulation run for an external electric field having strength $E_0 = 150$, frequency $\omega = 0$, $\Gamma = 2.5$, taking $\gamma = 7, 10$ and 20, with aspect ratio value $L_y = L_x$. The study is performed in the presence of the obstacle. From our study it is observed that γ influences the geometric structures of the lanes. The lane merging tendency decreases with increasing γ, which leads to an increase in the number of lanes and a decrease in lane width with increasing γ. The reason
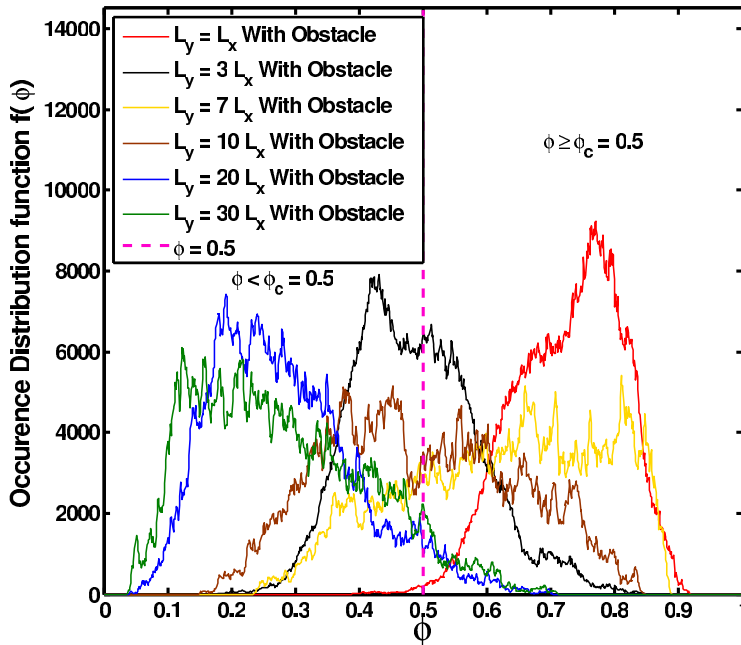
FIGURE 11. Occurrence distribution function of ϕ (or $f(\phi)$) versus instantaneous order parameter ϕ of the 2-D PIP system for constant ($\omega = 0$) external electric field in the presence of the obstacle is plotted by taking aspect ratio values $L_y = L_x$, $L_y = 3L_x$, $L_y = 7L_x$, $L_y = 10L_x$, $L_y = 20L_x$ and $L_y = 30L_x$. The other parameters used are $\Gamma = 2.5$, $E_0 = 150$.

behind this effect may be explained in terms of the PIP particles moving irregularly as their velocities are continuously damped away by friction and replaced by the random force. The motion can be thought of as a series of independent displacements taken at random, one after another. We would probably have guessed that a larger friction coefficient would lead to a smaller average displacement. This reduces the tendency of lanes to diffuse into each other perpendicular to the driven direction (i.e. Y direction). As a result of which thinner lanes are formed which also increases the lane count. Similar results are also observed in the presence of a time-varying electric field in both the presence and absence of the obstacle; however, results are not included in this study.

4.1.3. *Comparative study: without and with obstacle*

In this subsection, a comparative study to understand the lane stability in greater detail is performed in both the presence and absence of the obstacle, taking the same set of input parameters, i.e. $\Gamma = 2.5$, $E_0 = 150$, $\omega = 0$ and $\rho = 1.0$. As shown in figure 14, we have obtained ϕ versus $t\omega_{pd}$ plots for different aspect ratio values $L_y/L_x = 1, 3, 7, 10, 20$ and 30. Evidently, from the increasing fluctuations in the ϕ plot with increasing aspect ratio, it is clear that the stability of the lanes decreases in the presence of the obstacle and with an increase in aspect ratio value. Our observation is supported by the comparative $f(\phi)$ versus instantaneous ϕ plots (see figure 15), obtained using the same set of parameters as used in figure 14, in both the presence and absence of the obstacle. Figure 15 shows that with increasing value of the aspect ratio the $f(\phi)$ curve gradually shifts towards $\phi \leq 0.5$ domain, where the system starts to transition towards partially lane mixing phase. However, it is observed that the phase transition due to the mixing of lanes plays a dominating role in presence of an obstacle.
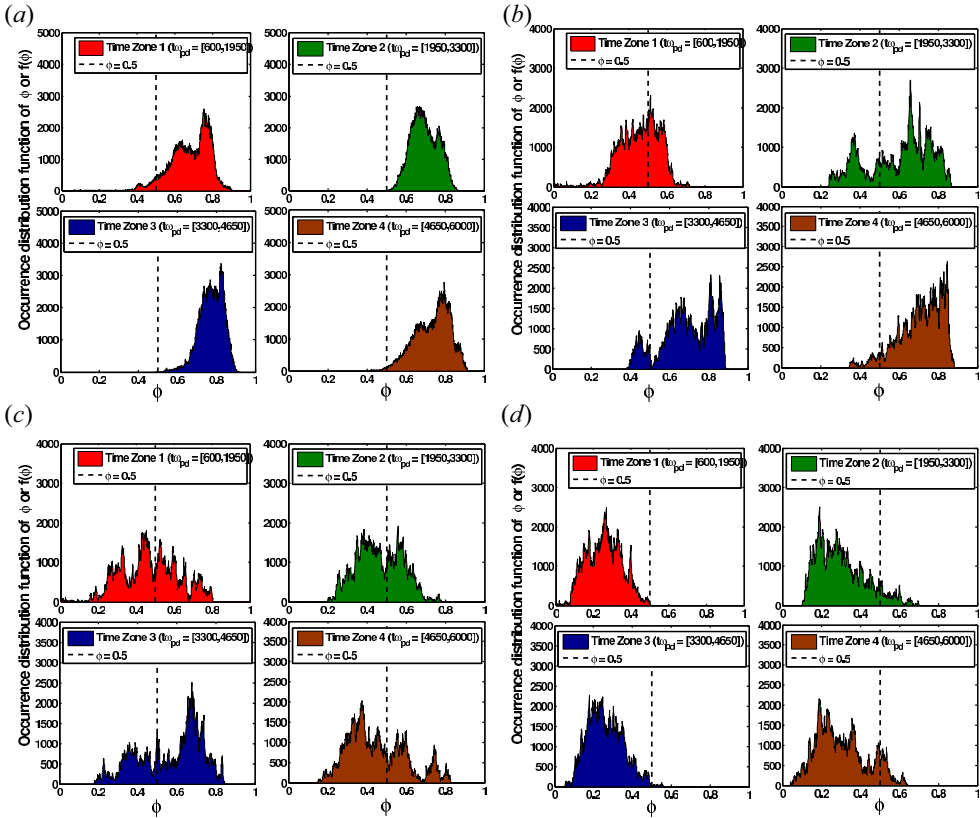
FIGURE 12. Occurrence distribution function of ϕ ($f(\phi)$) calculated for different geometric aspect ratio values (*a*) $L_y = L_x$, (*b*) $L_y = 7L_x$, (*c*) $L_y = 10L_x$ and (*d*) $L_y = 20L_x$, after turning on the external electric field at $t\omega_{pd} = 600$ simulation time step. The area under each curve is recorded for various simulation time zones of the 2-D PIP system for constant external electric field ($\omega = 0$) in presence of the obstacle. The other parameters used are $\Gamma = 2.5$, $E_0 = 150$, $\rho = 1.0$.
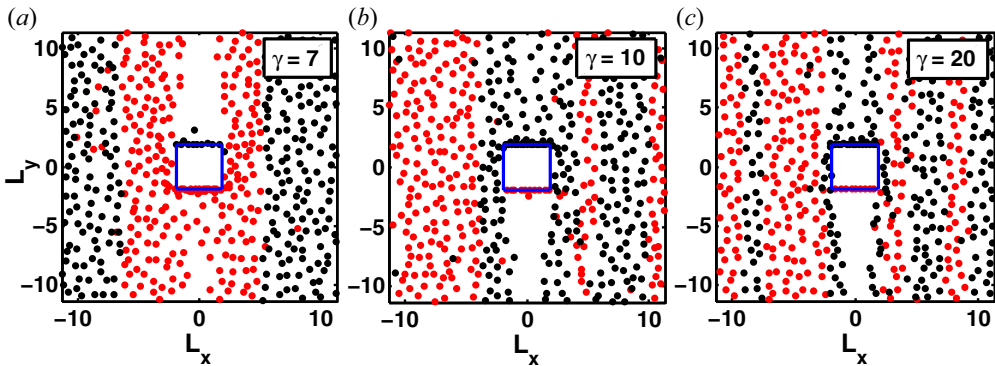
FIGURE 13. Typical simulation snapshots of the 2-D PIP system with constant external electric field ($\omega = 0$) in the presence of the obstacle are plotted by taking $\gamma = 7$, 10 and 20, with aspect ratio value $L_y = L_x$. The other parameters used are $\Gamma = 2.5$, $E_0 = 150$. Here, the external electric force $\boldsymbol{F}_E$ is applied along the Y direction.
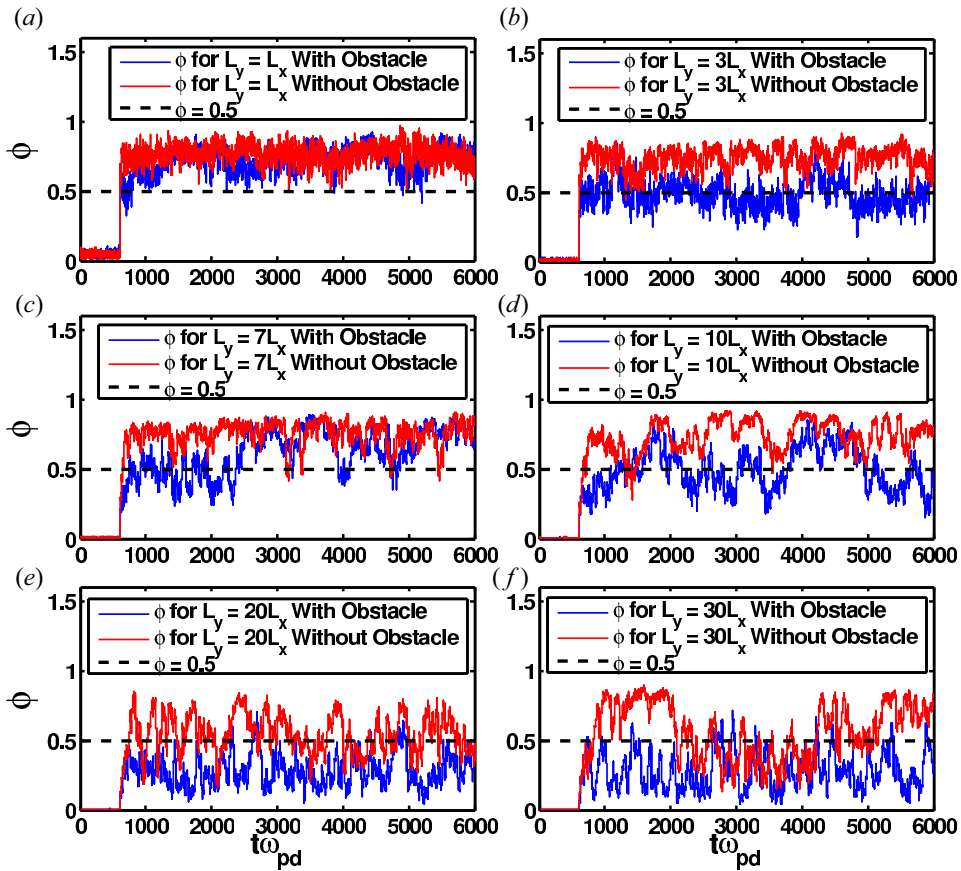
FIGURE 14. Comparative order parameter ϕ versus $t\omega_{pd}$ of the 2-D PIP system for constant ($\omega = 0$) external electric field in both the presence and absence of the obstacle is plotted by taking aspect ratio values (a) $L_y = L_x$, (b) $L_y = 3L_x$, (c) $L_y = 7L_x$, (d) $L_y = 10L_x$, (e) $L_y = 20L_x$ and (f) $L_y = 30L_x$. The other parameters used are $\Gamma = 2.5$, $\rho = 1.0$, $E_0 = 150$.

Analogous to the pedestrian theory, here the behaviour of the PIP particles can easily be understood by considering the motion of PIP particles inside the simulation chamber as a pedestrian flow in a corridor where the obstacle acts like a police officer responsible for the separation of pedestrians flowing in opposite directions. Like increasing the corridor length makes it difficult for the police official to maintain the flow separation throughout the corridor, which leads to a partially chaotic situation of pedestrians in which they are unable to maintain the flow in a lane structure formation, here in our study also with increasing the value of the geometric aspect ratio the PIP system moves towards a chaotic phase where the order parameter value becomes very low even in the presence of an electric field greater than the critical electric field strength.

In figure 16, comparative snapshots of the particles are plotted at the end of every simulation run showing the instantaneous particle positions in both the presence and absence of the obstacle, taking aspect ratio values $L_y/L_x = 1, 7$ and 30. The other parameters used are $E_0 = 150$, $\omega = 0$, $\Gamma = 2.5$ and $\kappa = 0.0001$. It is evident from figure 16 that lower aspect ratio promotes lane separation even in crowded situations, in both the presence and absence of the obstacle. However, as mentioned above, in the
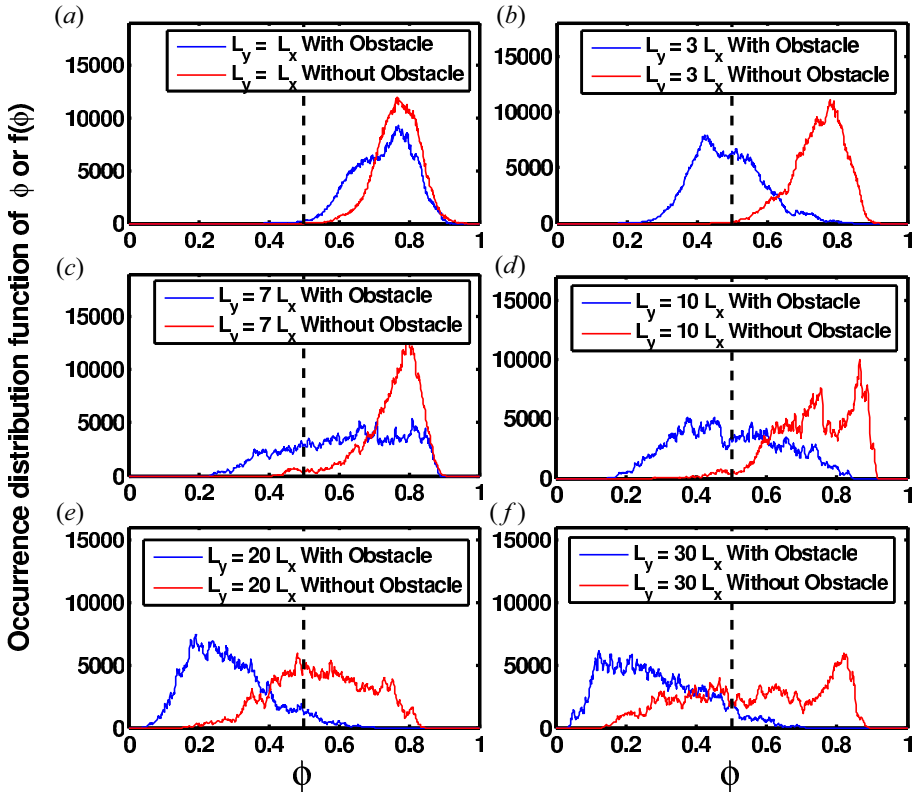
FIGURE 15. Comparative plots of occurrence distribution function of ϕ (or $f(\phi)$) versus instantaneous order parameter ϕ of the 2-D PIP system for constant ($\omega = 0$) external electric field in both the presence and absence of the obstacle taking aspect ratio values (*a*) $L_y = L_x$, (*b*) $L_y = 3L_x$, (*c*) $L_y = 7L_x$, (*d*) $L_y = 10L_x$, (*e*) $L_y = 20L_x$ and (*f*) $L_y = 30L_x$. The other parameters used are $\Gamma = 2.5$, $E_0 = 150$.

presence of both higher aspect ratio and obstacle, the system moves towards a chaotic phase where the order parameter value becomes very low even in the presence of an electric field greater than E_c. In other words, the obstacle tends to drive a transition of the PIP system towards a lane mixing phase at higher values of aspect ratio. Our observation is also supported by comparative $f(\phi)$ versus ϕ plots as shown in figure 15, which indicate that for lower aspect ratio the system remains in a lane state during the whole simulation time, in both the presence and absence of the obstacle; however, in the presence of the obstacle the PIP system completely transitions to a lane mixing state with $\phi < 0.5$ for $L_y/L_x \geq 20$. Further, from figure 16, in the presence of the obstacle the generation of a low-density region (which may be identified as a 'void') on either side of the obstacle is also observed for the system with low aspect ratio value. However, this void formation is not observed in our PIP system in the absence of the obstacle.

With the concept described above, the phase diagram for the PIP system in the presence of constant external electric field is plotted in figure 17. The location of the phase transition is estimated via the behaviour of the order parameter ϕ as a function of aspect ratio L_y/L_x in both the presence and absence of the obstacle. The other parameters used for this set of runs are $E_0 = 150$, $\omega = 0$ and $\Gamma = 2.5$. Figure 17 indicates that the value of the order parameter ϕ decreases gradually and goes beyond 0.5 with aspect ratio value $L_y/L_x \geq 9.0$
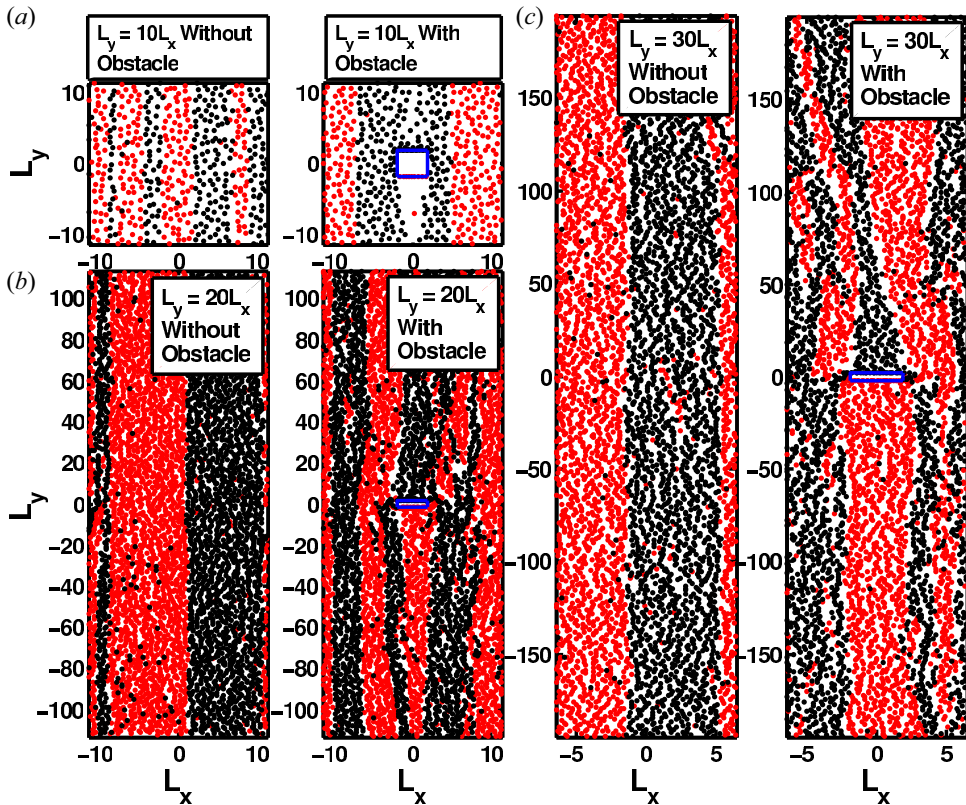
FIGURE 16. Typical comparative simulation snapshots of the 2-D PIP system with constant ($\omega = 0$) external electric field in both the presence and absence of the obstacle are plotted by taking aspect ratio values (*a*) $L_y = L_x$, (*b*) $L_y = 7L_x$, and (*c*) $L_y = 30L_x$. The other parameters used are $\Gamma = 2.5, E_0 = 150$. Here, the external electric force $\boldsymbol{F}_E$ is applied along the Y direction.

in the presence of the obstacle. As a result, the system starts to transition from ordered lane state to partially lane mixing state.

4.2. *Lane formation in the presence of oscillatory ($\omega \neq 0$) electric field*

In this subsection, we report on comprehensive simulation studies of lane formation in the PIP system that are carried out in the presence of an oscillatory external electric field. In particular, we focus on the influence of the obstacle and geometric aspect ratio on the lane dynamics. In this subsection, the entire work is performed using parameter values $\Gamma = 2.5, \rho = 1.0, E_0 = 150$ and $\omega = 0.001, 0.01$ and geometric aspect ratio value ranges from $L_y/L_x = 1$ to 40.

4.2.1. *Without obstacle*

In figure 18 the time variation of the order parameter values in the presence of the oscillatory external electric field having strength $E_0 = 150$ and frequency $\omega = 0.001, 0.01$ is plotted in the absence of the obstacle, taking different values of aspect ratio $L_y/L_x=$ 2, 3, 7, 10, 20 and 30. From the figure, it is observed that the oscillatory nature of the order parameter curve is consistent with the results obtained in our previous work (Sarma *et al.* 2020) for both values of frequency, which indicates that spontaneous formation and breaking of lane formation dynamics takes place in the case of the oscillating external
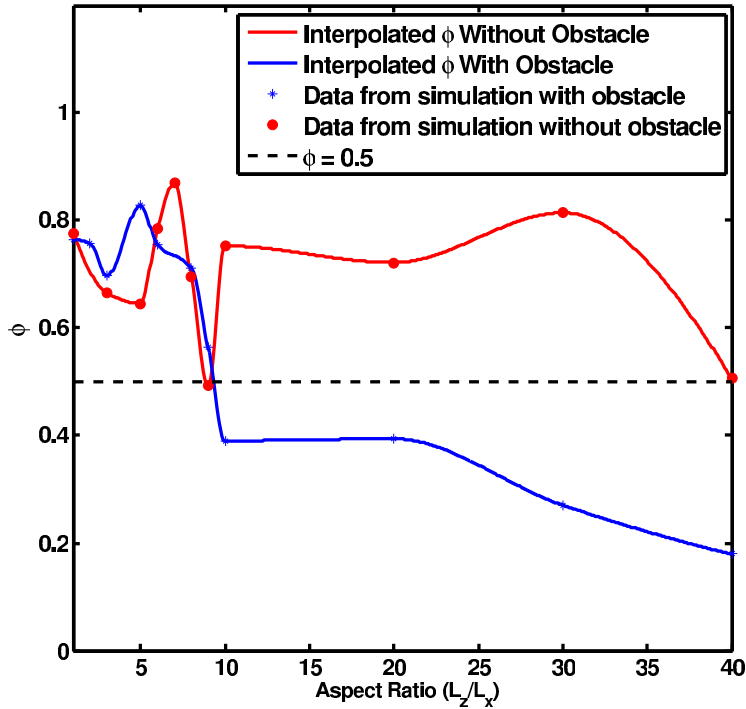
FIGURE 17. Comparative plot of order parameter ϕ versus aspect ratio L_y/L_x of the 2-D PIP system with constant ($\omega = 0$) external electric field in both the presence and absence of the obstacle. The other parameters used are $\Gamma = 2.5$, $E_0 = 150$.

electric field. It is seen that the effect of this spontaneous formation and breaking of lanes is independent of the geometric aspect ratio values (L_y/L_x). It is also observed that the excitation field frequency and the frequency that characterizes the time variation of the order parameter are roughly equal. However, due to the oscillatory nature of the applied electric field the lane merging tendency reduces significantly with increasing aspect ratio values. The lanes try to merge; however, the changing polarity of the oscillatory electric field in every half-cycle of oscillation hinders the merging of lanes which is very evident in the simulation snapshot (plotted for $\omega = 0.01$ only) provided in figure 19. The results in figure 19 are plotted in the absence of the obstacle; however, the simulation snapshots are recorded at the end of every simulation run (i.e. at $t\omega_{pd} = 6000$) and other input parameters are the same as used in the case of figure 18.

4.2.2. *With obstacle*

Here, the time variation of the order parameter (see figure 20) for the PIP system is studied with the obstacle in the presence of an external oscillatory electric field. Here, the order parameter is calculated taking aspect ratio values $L_y = 2L_x$, $L_y = 3L_x$, $L_y = 7L_x$, $L_y = 10L_x$, $L_y = 20L_x$ and $L_y = 30L_x$. The other parameters used are $E_0 = 150$ and $\omega = 0.001, 0.01$. Figure 20 indicates that an increasing value of the geometric aspect ratio has a significant effect on the order parameter values and this effect is invariant with the frequency of the applied electric field. With higher aspect ratio the stability of lanes decreases with decreasing order parameter value beyond $\phi = 0.5$. The related particle snapshots are plotted as shown in figure 20 for $\omega = 0.01$ only. Figure 20 shows that the mixing of lanes starts for aspect ratio value $L_y/L_x \geq 7.0$ in the presence of
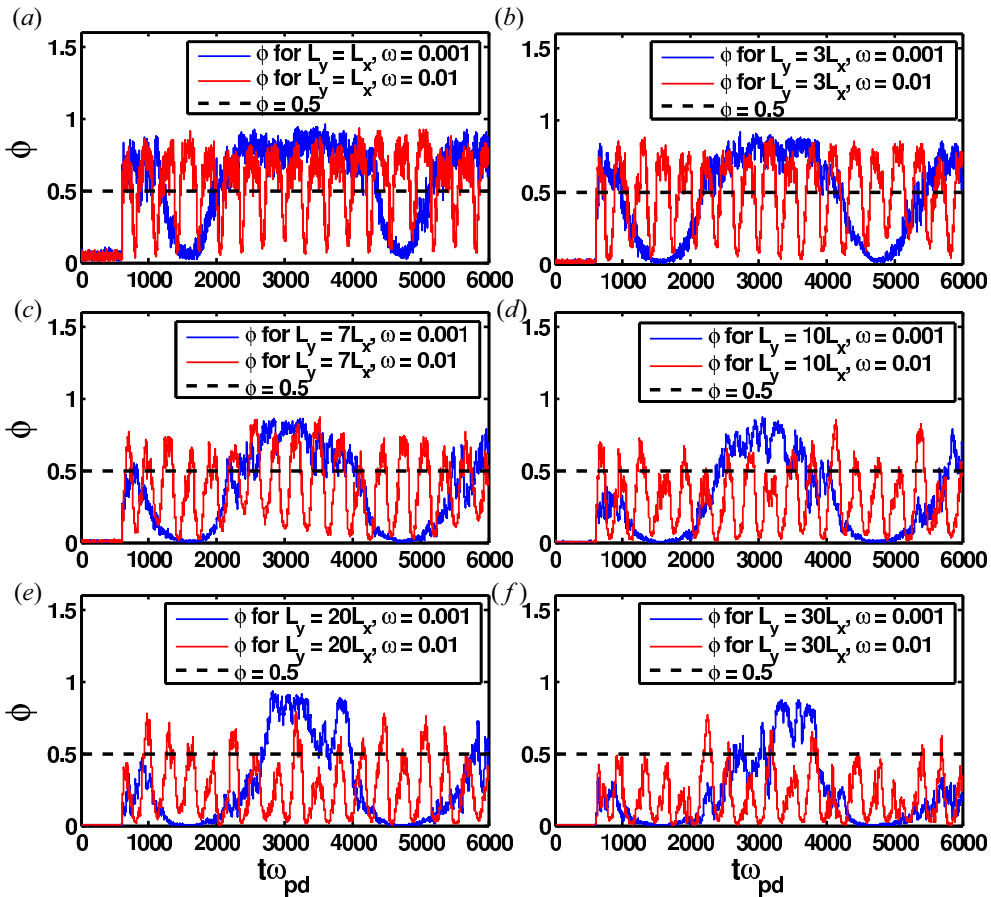
FIGURE 18. Order parameter ϕ versus $t\omega_{pd}$ of the 2-D PIP system for oscillatory external electric field ($\omega \neq 0$) in the absence of the obstacle is plotted by taking aspect ratio values (a) $L_y = L_x$, (b) $L_y = 3L_x$, (c) $L_y = 7L_x$, (d) $L_y = 10L_x$, (e) $L_y = 20L_x$ and (f) $L_y = 30L_x$. The other parameters used are $\Gamma = 2.5$, $E_0 = 150$, $\omega = 0.001, 0.01$.

the obstacle. However, the same phenomenon is observed for $L_y/L_x \geq 9.0$ (although related snapshots are not included) with $\omega = 0.001$ in the presence of the obstacle. This indicates that geometric aspect ratio values $L_y/L_x = 7, 9$ act as a transition point towards partial lane mixing phase in the presence of the obstacle taking $\omega = 0.01, 0.001$, respectively. Our study also reveals that as already observed in the presence of a constant electric field with the obstacle, here, in the case of oscillatory electric field, also the presence of the obstacle at the centre of the simulation box creates a void on either side of the obstacle. This void formation is only observed for lower values of the geometric aspect ratio (see figure 21). However, the PIP particles with charge opposite to that of the particles constituting the lanes always try to fill up this low-pressure area, which is very prominent at higher values of the aspect ratio ($L_y/L_x \geq 9$) as shown in figure 21.

4.3. *Lane formation dynamics in both presence ($\beta \neq 0$) and absence ($\beta = 0$) of external magnetic field*

In this subsection, the results obtained from a comparative study performed on lane formation dynamics in both the presence and absence of the external magnetic field
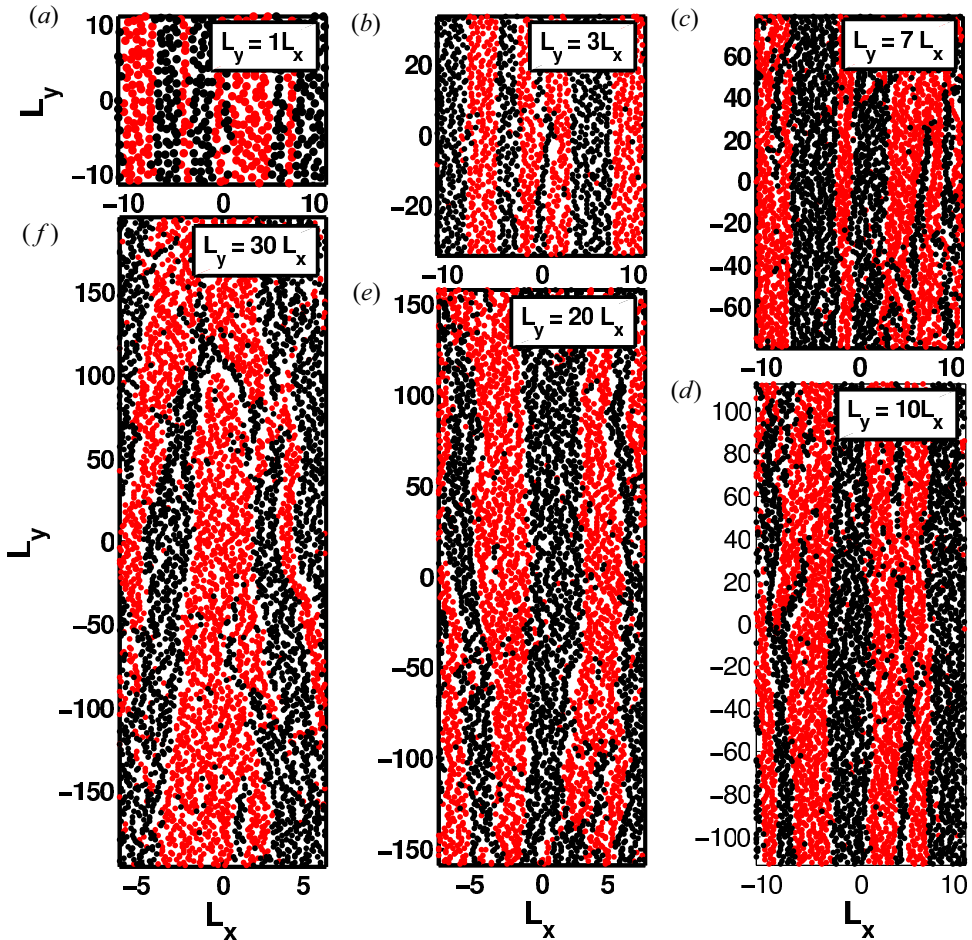
FIGURE 19. Typical simulation snapshots of the 2-D PIP system with oscillatory external electric field ($\omega \neq 0$) in the absence of the obstacle are plotted by taking aspect ratio values (*a*) $L_y = L_x$, (*b*) $L_y = 3L_x$, (*c*) $L_y = 7L_x$, (*d*) $L_y = 10L_x$, (*e*) $L_y = 20L_x$ and (*f*) $L_y = 30L_x$. The other parameters used are $\Gamma = 2.5$, $E_0 = 150$, $\omega = 0.01$. Here, the external electric force $\boldsymbol{F_E}$ is applied along the *Y* direction.

are investigated. In particular, we have examined the effect of geometric aspect ratio and obstacle on lane formation. This study has been performed in both the presence and absence of a time-varying external electric field. We have systematically examined the lane formation dynamics with different values of the geometric aspect ratio varying from $L_y/L_x = 1.0$ to 40 (although results for only a few values are mentioned here).

Our study reveals that the PIP system shows a kind of non-equilibrium lane formation dynamics in the presence of the external magnetic field similar to that shown in the absence of it. We perform our study by applying the external electric field (both constant and oscillatory) in the *Y* direction, considering the external magnetic field direction is out of the simulation chamber. As mentioned in our recent works on lane formation dynamics (Sarma *et al.* 2020; Baruah *et al.* 2021), here also it is observed that in the presence of the external magnetic field a critical value of the electric field strength exists above which lanes are formed distinctly. Like our earlier study (Baruah *et al.* 2021), we also observed
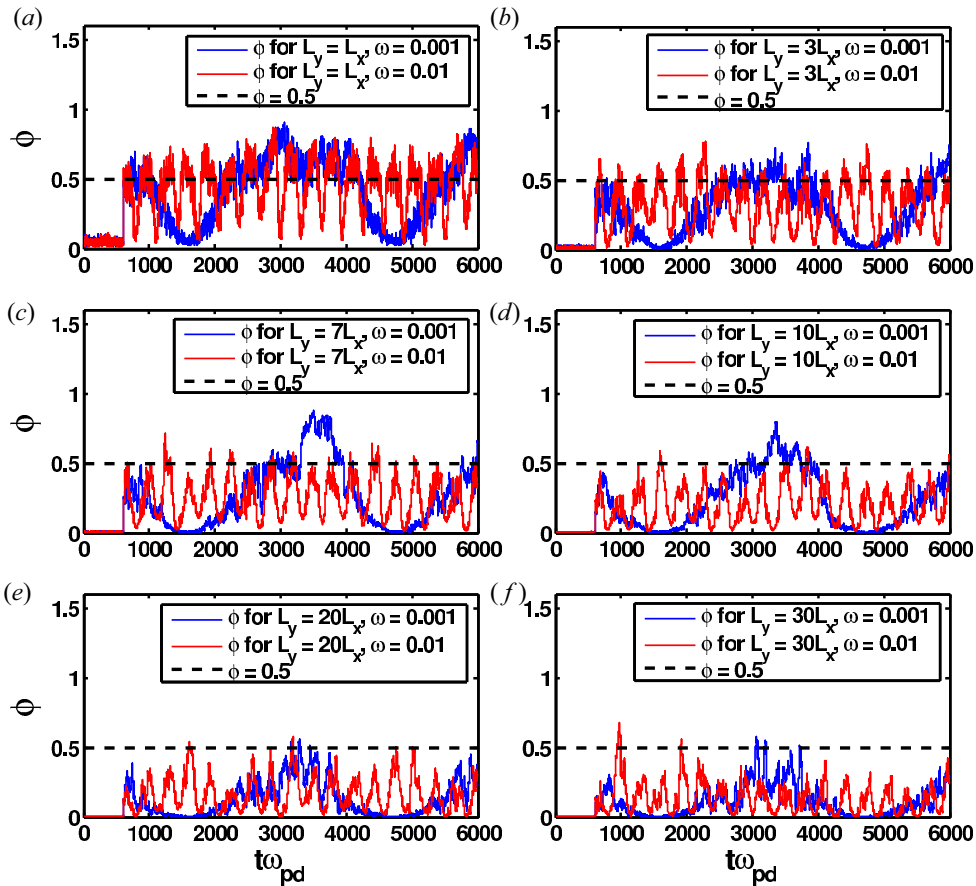
FIGURE 20. Order parameter ϕ versus $t\omega_{pd}$ of the 2-D PIP system for oscillatory external electric field ($\omega \neq 0$) in the presence of the obstacle is plotted by taking aspect ratio values (a) $L_y = L_x$, (b) $L_y = 3L_x$, (c) $L_y = 7L_x$, (d) $L_y = 10L_x$, (e) $L_y = 20L_x$ and (f) $L_y = 30L_x$. The other parameters used are $\Gamma = 2.5$, $\rho = 1.0$, $E_0 = 150$, $\omega = 0.001, 0.01$.

that the self-organized lanes start to move along a direction perpendicular to the directions of both the applied electric and magnetic fields due to the appearance of electric field drift (i.e. $E \times B$ drift) in our system. Further, in the presence of the external magnetic field our system also shows a non-stationary lane-like self-organization behaviour, with oscillation between self-organized and partial lane mixing states when submitted to a time-varying electric field in the absence of magnetic field. However, due to the similarity of the observations described above to our previous observations (Sarma *et al.* 2020; Baruah *et al.* 2021) in the field of lane formation dynamics, the relevant plots obtained in the presence of the external magnetic field are not mentioned here.

In order to investigate the dependence of non-equilibrium lane formation dynamics on the magnetic field strength, instantaneous lane order parameter is recorded as a function geometric aspect ratio, as shown in both the presence and absence of external magnetic field in figure 22. The study is performed by taking a constant external electric field with the obstacle. While ϕ is large for smaller aspect ratio values, it decays when a critical value of the aspect ratio is approached. The resulting critical value of geometric aspect ratio thus obtained is then compared with the one in the absence of the external magnetic field and it
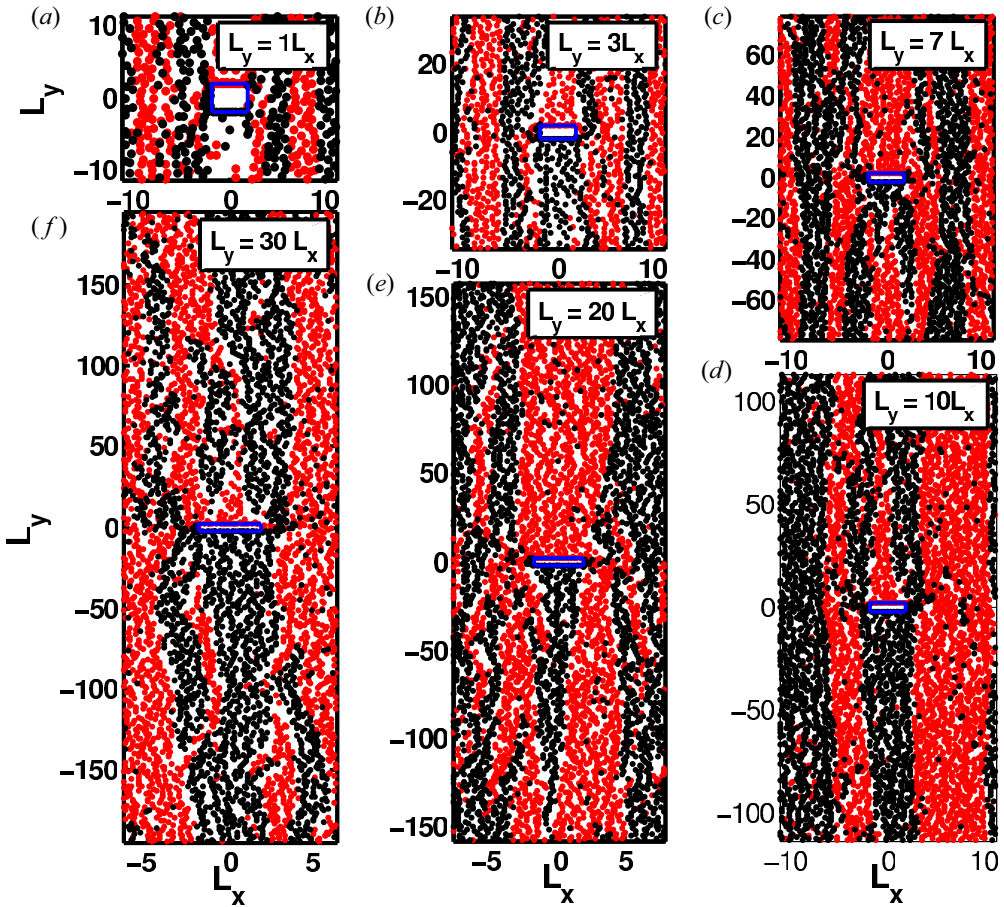
FIGURE 21. Typical simulation snapshots of the 2-D PIP system with oscillatory external electric field ($\omega = 0.01$) in the presence of the obstacle are plotted by taking aspect ratio values (a) $L_y = L_x$, (b) $L_y = 3L_x$, (c) $L_y = 7L_x$, (d) $L_y = 10L_x$, (e) $L_y = 20L_x$ and (f) $L_y = 30L_x$. The other parameters used are $E = 150$, $\Gamma = 2.5$. Here, the external electric force $\boldsymbol{F}_E$ is applied along the Y direction.

is observed that the presence of the external magnetic field accelerates the phase transition process and leads to a lane mixing phase in the presence of the obstacle.

Simulation snapshots associated with a situation with a constant external electric field ($\omega = 0$) in the presence of the obstacle, recorded at different simulation times, are shown in figure 23(a). The related plot of instantaneous ϕ as a function of time t is shown in figure 23(b). The corresponding simulation times when the snapshots are recorded, as shown in figure 23(a), are indicated by vertical lines in figure 23(b). The study is done in the presence of an external magnetic field with $\beta = 0.1$ taking aspect ratio value $L_y = 2L_x$. Here, the external electric force $\boldsymbol{F}_E$ is applied along the Y direction. One clearly sees lane formation parallel to the external electric field. In the snapshots, formation of a void-like region on the side of the obstacle is observed also in presence of the external magnetic field. Our study also reveals that this void-like region looks more prominent for lower value of aspect ratio. Further, in the presence of an external magnetic field only, the flipping of voids in irregular intervals is observed on both sides of the obstacle. From our analysis
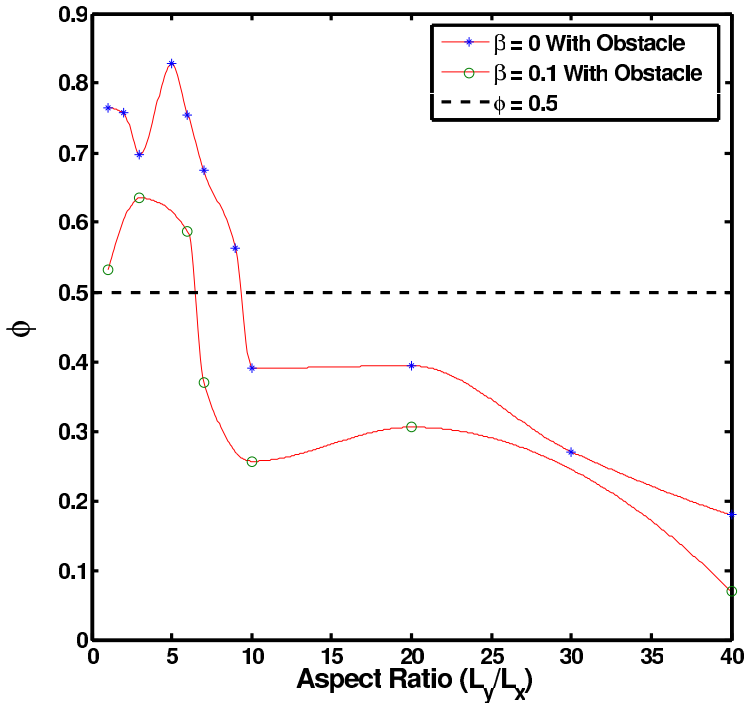
FIGURE 22. Comparative order parameter ϕ versus aspect ratio L_y/L_x plot of the 2-D PIP system in both the presence and absence of external magnetic field with obstacle. The other parameters used are $\beta = 0.1$, $\Gamma = 2.5$, $E_0 = 150$, $\omega = 0$.

it is observed that the interval between this flipping is dependent on the thickness of the formed lanes. Wider lanes result in a larger interval between the flipping of voids, which in turn reduces the frequency of this flipping. It may be said that the observed frequency of the flipping is inversely proportional to the thickness of the lanes. Additionally, it is noticed that a lane having thickness greater than the thickness of the obstacle is required to flip the voids. This flipping of voids in the presence of an external magnetic field is also observed when a time-dependent electric field is applied to the system. However, the related snapshots are not included in this work.

The flipping of voids may be due to the drift of the lanes in the presence of the external magnetic field caused by $E \times B$ drift in a direction perpendicular to both applied electric field (along Y axis) and magnetic field (along negative Z axis). The direction of this $E \times B$ drift is observed along the negative X axis. This drift can be seen in figure 24(*a*) where progressive simulation snapshots are shown for $L_y/L_x = 3$ in the presence of both external electric and magnetic fields when the obstacle is present. Any particular lane can be observed to have a drift along the X axis. For ease of consideration, figure 24(*a*) highlights a lane of positively charged (red) particles bounded within two blue dashed lines and running positions of that particular bunch of PIP particles with time are noticed here. The initial snapshot is taken at $t\omega_{pd} = 2802$ and the position of the lane is bounded within $L_x = -3.807$ and 8.984. The next snapshot is taken at $t\omega_{pd} = 2832$ where the highlighted lane is displaced in the negative X direction. This is evident from the displacement of the lower and upper bound of the lane boundary which are at $L_x = -4.590$ and 6.817, respectively. The next snapshot is taken at $t\omega_{pd} = 2873$ where the lane is further displaced with its lower and upper bound being at $L_x = -6.451$ and 3.596. Here the average velocity vector for the
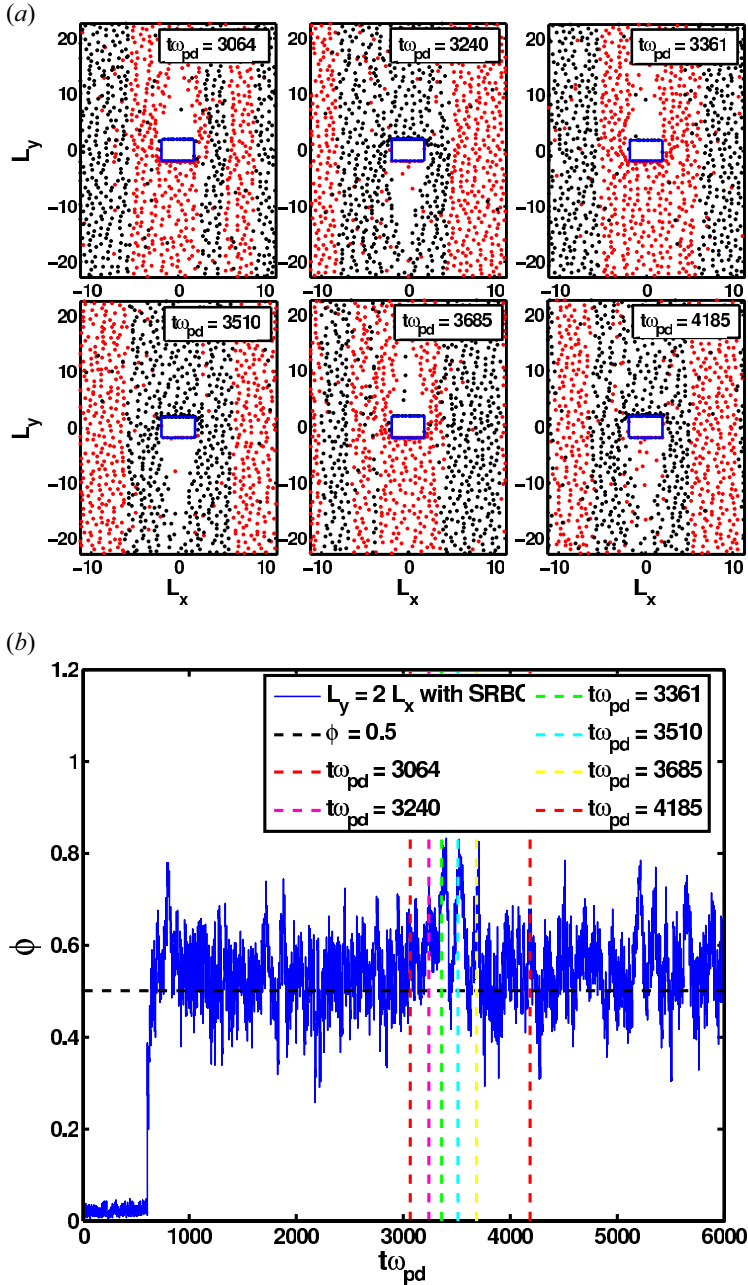
FIGURE 23. (*a*) Typical simulation snapshots of the 2-D PIP system in the presence of constant external electric field ($\omega = 0$) with the obstacle are plotted at different simulation time steps. The study is done in the presence of external magnetic field with $\beta = 0.1$. Here, the external electric force is applied along the Y direction. The other parameters used are $\Gamma = 2.5$, $E_0 = 150$, $\omega = 0.0$. (*b*) Order parameter ϕ versus $t\omega_{pd}$ plot of the 2-D PIP system with constant external electric field ($\omega = 0$) with the obstacle. The snapshots recorded at different simulation times are shown in figure 21. The study is done in the presence of external magnetic field with $\beta = 0.1$. The other parameters used are $\Gamma = 2.5$, $E_0 = 150$, $\omega = 0$.
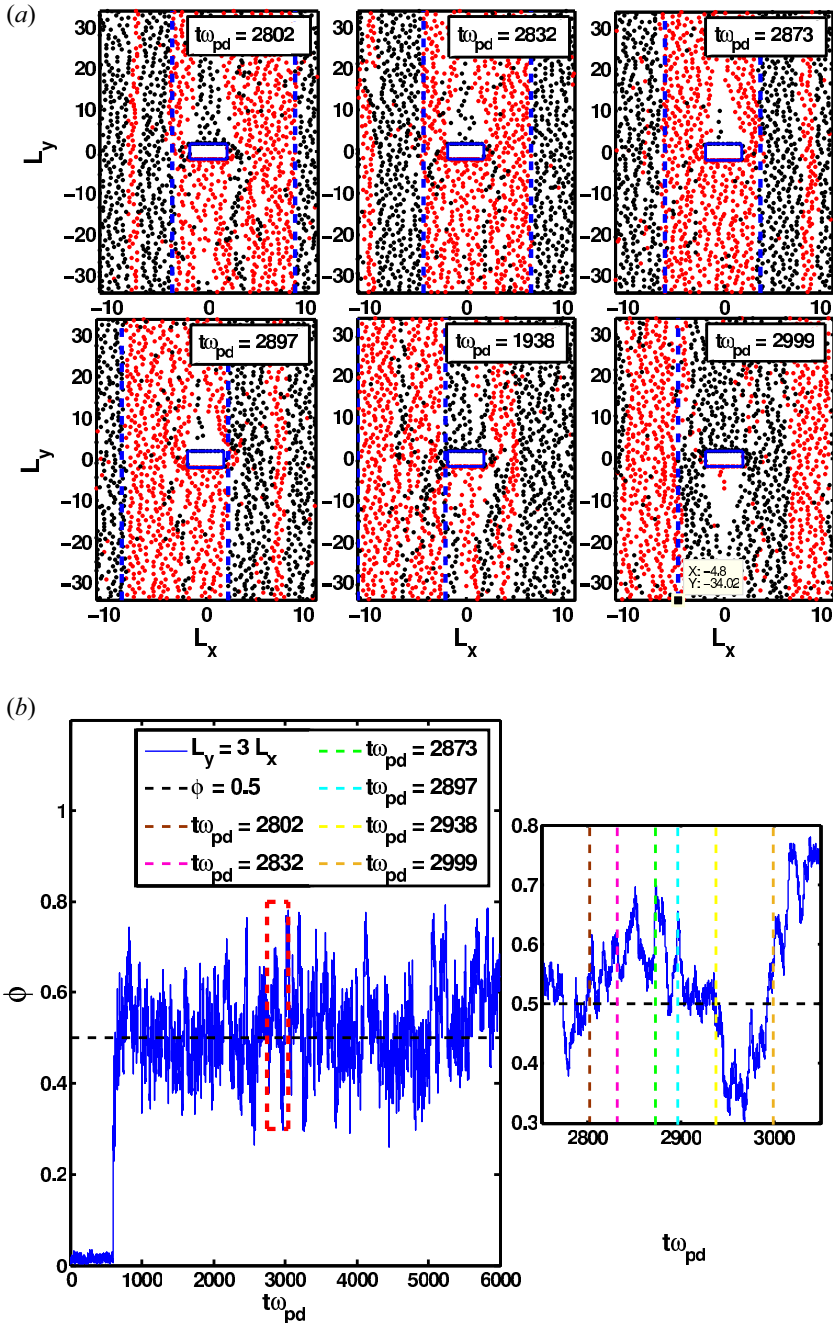
FIGURE 24. (*a*) Typical simulation snapshots of the 2-D PIP system in the presence of constant external electric field ($\omega = 0$) with obstacle are plotted at different simulation time steps. To denote a lane consisting of positive (red-coloured) PIP particles, two blue dashed lines are used and instantaneous positions of that particular lane with time are noted, which indicates the presence of $E \times B$ drift. (*b*) Order parameter ϕ versus $t\omega_{pd}$ plot corresponding to (*a*). The right-hand panel is a zoomed plot from $t\omega_{pd} = 2500$ to 3500. The snapshots recorded at different simulation times are shown in (*a*). The study is done in the presence of the external magnetic field with $\beta = 0.1$. Here, the external electric force is applied along the Y direction. The other parameters used are $\Gamma = 2.5$, $E_0 = 150$, $\omega = 0$.
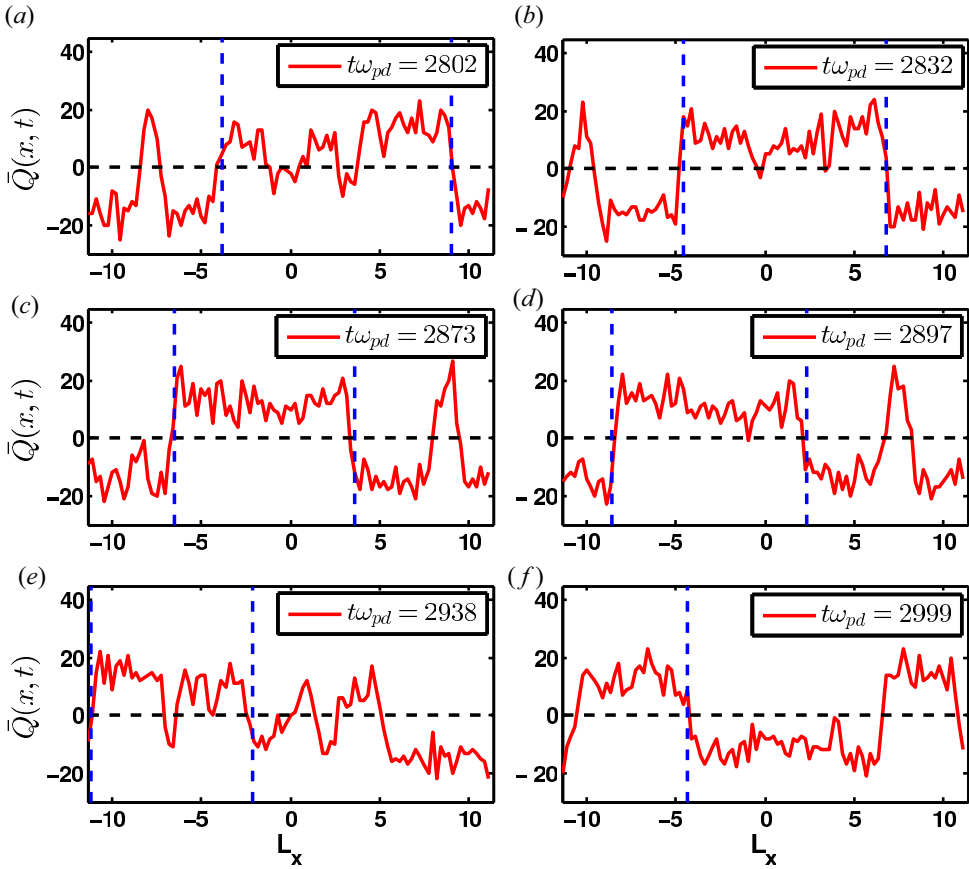
FIGURE 25. The *Y*-averaged charge profile $\bar{Q}(x)$ is plotted corresponding to the instantaneous particle snapshots recorded in figure 24(*a*), at (*a*) $t\omega_{pd} = 2802$, (*b*) $t\omega_{pd} = 2832$, (*c*) $t\omega_{pd} = 2873$, (*d*) $t\omega_{pd} = 2897$, (*e*) $t\omega_{pd} = 2938$ and (*f*) $t\omega_{pd} = 2999$. The parameters used are $\Gamma = 2.5$, $E_0 = 150$, $\omega = 0$, $\beta = 0.1$ and $L_y/L_x = 3$.

positively charged particles points upwards (positive *Y* axis). As a result of which a void is formed beside the obstacle as the flow of particles is being obstructed by it. Two further snapshots are taken at $t\omega_{pd} = 2897$ and 1938 which show further displacement of the lane in the same negative *X* direction. The last snapshot is taken at $t\omega_{pd} = 2999$ where the lane is displaced and approaches the boundary of the simulation cell. Simultaneously, the lane of negatively charged particles beside the highlighted lane has engulfed the obstacle. The average velocity vector of the negatively charged (black) particles is opposite (i.e. along negative *Y* axis) to that of the positively charged particles. This opposite flow causes the void to form on the opposite side of the obstacle, thus flipping the side on which the void was formed earlier. The corresponding order parameter plot is shown in figure 24(*b*). The right-hand panel is a zoomed plot from $t\omega_{pd} = 2500$ to 3500 and the vertical lines within the plot denote the corresponding time when snapshots shown in figure 24(*a*) are recorded. It can be seen that $E \times B$ drift contributes to the fluctuations in the order parameter values accompanied by flipping of voids.

Figure 25 shows the *Y*-averaged charge profile, corresponding to figure 24(*a*), measured at $t\omega_{pd} = 2802, 2832, 2873, 2897, 2938$ and 2999. The peaks with positive

values represent the lanes formed by positively charged particles. The lane previously highlighted in figure 24(*a*) is also indicated here in figure 25 by bounding with blue lines. The $E \times B$ drift along the negative X direction is evident from this diagnostic technique as well. In figure 25, the profile of positive lane bounded by blue lines is seen to move towards the left. At $t\omega_{pd} = 2802$, the position of the extreme right-hand layer of the lane formed by the positive (red) PIP particles (bounded by blue line) is recorded as $L_x = 8.984$ (see figure 25*a*), which shifted to $L_x = 6.817$ at $t\omega_{pd} = 2832$ (see figure 25*b*) followed by $L_x = 3.596$ at $t\omega_{pd} = 2873$ (see figure 25*c*), $L_x = 2.365$ at $t\omega_{pd} = 2897$ (see figure 25*d*), $L_x = -2.147$ at $t\omega_{pd} = 2938$ (see figure 25*e*) and $L_x = -4.310$ at $t\omega_{pd} = 2999$ (see figure 25*f*). These values indicate that there is a drift of lanes along a direction perpendicular to the directions of both applied electric and magnetic fields. Notably, this drift is not observed in the absence of external magnetic field.

5. Conclusions

From the study performed for addressing the effect of obstacle and geometric aspect ratio on lane formation dynamics in a 2-D PIP system with under-damped limit using the Langevin dynamics simulation technique, we can draw the following conclusions:

(i) Electric field greater than some critical threshold field strength establishes self-organization leading to lane formation. However, the critical value of the electric field E_c, and hence the location of the phase transition, is affected by the Coulomb coupling parameter, i.e. Γ, value (although results other than those for $\Gamma = 2.5$ are not mentioned here). By increasing (decreasing) the value of Γ the correlation between the PIP particles is strengthened (weakened), so as a conclusive result we can state that whenever the correlation is increased (decreased) the critical force becomes higher (lower). For increasing (decreasing) interaction energy by increasing (decreasing) the value of Γ, an enhanced (diminished) E_c is necessary to drive a transition towards lane formation.

(ii) It is observed that during lane formation, the friction constant plays a significant role in the geometric structure of the lanes.

(iii) Geometric aspect ratio plays an important role in the stability of the lanes formed. The number of lanes per species decreases with increasing aspect ratio in the absence of an obstacle because of merging of similar species of particles in the system due to the elongated corridor available for the flow at higher aspect ratio values.

(iv) The higher the aspect ratio, the less stable is the lane formed. Older lanes are readily broken due to the friction at the separation boundary of two oppositely flowing lanes, and newer lanes are formed subsequently.

(v) The presence of an obstacle further promotes the merging of lanes, and the system gradually transitions to a partially mixed phase with higher value of aspect ratio.

(vi) It is also observed that the PIP particle flow is obstructed by the obstacle resulting in the formation of a void which in turn attracts particles with polarity opposite to that of the particles due to which the void was created.

(vii) When the obstacle is present, the merging of lanes is prominent even for low aspect ratio value. However, at higher aspect ratio values very few stable lanes are formed and the system remains below $\phi = 0.5$ for almost the whole simulation time.

(viii) In the presence of an external oscillating electric field, spontaneous breaking of lane formation is observed due to the oscillatory nature of the applied field and is dependent on the frequency of the oscillation of the applied field.

(ix) For the oscillatory field case, at higher aspect ratio values the presence of an obstacle further reduces the value of ϕ to such an extent that the order parameter value no longer exceeds 0.5, i.e $\phi \leq 0.5$, and the system stays in a partial disordered state.

Finally, a comparative study of the effect of aspect ratio and obstacle on the lane formation dynamics in both the presence and absence of an external magnetic field for the PIP system reveals the following:

(i) The presence of the external magnetic field in the PIP system with an obstacle accelerates the phase transition process and leads to a lane mixing phase.

(ii) Our investigation demonstrates that due to the presence of both electric and magnetic fields, the PIP particles experience ($E \times B$) drift which occurs in the form of fluctuations in the order parameter plot in a strongly coupled regime for the presence of both constant and oscillatory external electric fields. The lanes are found to move along a direction perpendicular to the both E and B field directions as a result of the guiding centre drift.

(iii) In the presence of magnetic field, flipping of voids in irregular intervals is observed on both sides of the obstacle, which is observed in the presence of both constant and time-varying electric fields.

Finally, we have reported the effect of aspect ratio on lane formation dynamics in a driven PIP system in the presence of an obstacle. Our simulation results may help to identify the parameter range of lane formation phase in such kinds of systems to a large extent.

Declaration of interests

The authors report no conflict of interest.

Data availability statement

The data that support the findings of this study are available from the corresponding author upon reasonable request.

Author contributions

S.B. and R.G. prepared the theoretical model. All authors contributed equally in performing the simulations, analysing data, reaching conclusions and writing the paper.

REFERENCES

ABDELSALAM, U. 2010 Dust-ion-acoustic solitary waves in a dense pair-ion plasma. *Physica* B **405** (18), 3914–3918.

ARSHAD, K. & MAHMOOD, S. 2010 Electrostatic ion waves in non-maxwellian pair-ion plasmas. *Phys. Plasmas* **17** (12), 124501.

BARUAH, S., GANESH, R. & AVINASH, K. 2015 A molecular dynamics study of phase transition in strongly coupled pair-ion plasmas. *Phys. Plasmas* **22** (8), 082116.

BARUAH, S., SARMA, U. & GANESH, R. 2021 Effect of external magnetic field on lane formation in driven pair-ion plasmas. *J. Plasma Phys.* **87** (2), 905870202.

CHEN, F. F. 2016 *Introduction to Plasma Physics and Controlled Fusion*, 3rd edn. Springer.

DWIVEDI, C. 2000 Dynamo transformation of the collisional R-T in a weakly ionized plasma. *Pramana J. Phys.* **55** (5–6), 849–854.

FELICIANI, C., MURAKAMI, H. & NISHINARI, K. 2018 A universal function for capacity of bidirectional pedestrian streams: filling the gaps in the literature. *PLoS ONE* **13**, e0208496.

IKEDA, K. & KIM, K. 2017 Lane formation dynamics of oppositely self-driven binary particles: effects of density and finite system size. *J. Phys. Soc. Japan* **86** (4), 044004.

KIM, S.-H., HEINRICH, J. & MERLINO, R. 2008 Electrostatic ion-cyclotron waves in a plasma with heavy negative ions. *Planet. Space Sci.* **56** (11), 1552–1559.

KIM, S.-H. & MERLINO, R. L. 2007 Electron attachment to c_7f_14 and sf_6 in a thermally ionized potassium plasma. *Phys. Rev. E* **76**, 035401.

KIM, S. H., MERLINO, R. L., MEYER, J. K., ROSENBERG, M. 2013 Low-frequency electrostatic waves in a magnetized, current-free, heavy negative ion plasma. *J. Plasma Phys.* **79** (6), 1107–1111.

KOGLER, F. & KLAPP, S. 2015 Lane formation in a system of dipolar microswimmers. *Europhys. Lett.* **110**.

MAHAJAN, S. M. & SHATASHVILI, N. L. 2008 Wave localization and density bunching in pair ion plasmas. *Phys. Plasmas* **15** (10), 100701.

NETZ, R. R. 2003 Conduction and diffusion in two-dimensional electrolytes. *Europhys. Lett.* **63** (4), 616–622.

OOHARA, W., DATE, D. & HATAKEYAMA, R. 2005 Electrostatic waves in a paired fullerene-ion plasma. *Phys. Rev. Lett.* **95**, 175003.

OOHARA, W., FUJII, M., WATAI, M., HIRAOKA, Y., EGAWA, M., MORINAGA, Y., TAKAMORI, S. & YOSHIDA, M. 2019 Generation of hydrogen ionic plasma superimposed with positive ion beam. *AIP Adv.* **9** (8), 085303.

OOHARA, W. & HATAKEYAMA, R. 2003 Pair-ion plasma generation and fullerene-dimer formation. *Thin Solid Films* **435**, 280–284.

OOHARA, W. & HATAKEYAMA, R. 2007 Basic studies of the generation and collective motion of pair-ion plasmas. *Phys. Plasmas* **14** (5), 055704.

PIRAN, T. 2005 The physics of gamma-ray bursts. *Rev. Mod. Phys.* **76**, 1143–1210.

SALEEM, H. 2006 Kinetic theory of acoustic wave in pair-ion plasmas. *Phys. Plasmas* **13** (4), 044502.

SALEEM, H. 2007 A criterion for pure pair-ion plasmas and the role of quasineutrality in nonlinear dynamics. *Phys. Plasmas* **14** (1), 014505.

SALEEM, H., VRANJES, J. & POEDTS, S. 2006 On some properties of linear and nonlinear waves in pair-ion plasmas. *Phys. Lett.* A **350** (5), 375–379.

SARMA, U., BARUAH, S. & GANESH, R. 2020 Lane formation in driven pair-ion plasmas. *Phys. Plasmas* **27** (1), 012106.

SCHMITTMANN, B. & ZIA, R. 1998 Driven diffusive systems. An introduction and recent developments. *Phys. Rep.* **301** (1), 45–64.

SHUKLA, P. K. & STENFLO, L. 2005 Periodic structures on an ionic-plasma-vacuum interface. *Phys. Plasmas* **12** (4), 044503.

TARAMA, S., EGELHAAF, S. U. & LÖWEN, H. 2019 Traveling band formation in feedback-driven colloids. *Phys. Rev.* E **100**, 022609.

TRIBECHE, M., GOUGAM, L. A., BOUBAKOUR, N. & ZERGUINI, T. H. 2007 Electrostatic solitary structures in a charge-varying pair–ion–dust plasma. *J. Plasma Phys.* **73** (3), 403–415.

VERHEEST, F. 2006 Existence of bulk acoustic modes in pair plasmas. *Phys. Plasmas* **13** (8), 082301.

VISSERS, T., VAN BLAADEREN, A. & IMHOF, A. 2011*a* Band formation in mixtures of oppositely charged colloids driven by an ac electric field. *Phys. Rev. Lett.* **106**, 228303.

VISSERS, T., WYSOCKI, A., REX, M., LÖWEN, H., ROYALL, C. P., IMHOF, A. & VAN BLAADEREN, A. 2011b Lane formation in driven mixtures of oppositely charged colloids. *Soft Matt.* **7**, 2352–2356.

VLADIMIROV, S., OSTRIKOV, K., YU, M. & MORFILL, G. 2003 Ion-acoustic waves in a complex plasma with negative ions. *Phys. Rev.* E **67**, 036406.

VRANJES, J. & POEDTS, S. 2005 On waves and instabilities in pair-ion plasma. *Plasma Sources Sci. Technol.* **14** (3), 485–491.